Cell Chemical Biology

CellPress

Review

# Lanthanide-Based Optical Probes of Biological Systems

Ukrae Cho[1,4,*] and James K. Chen[1,2,3,*]
[1]Department of Chemical and Systems Biology, Stanford University, Stanford, CA 94305, USA
[2]Department of Developmental Biology, Stanford University, Stanford, CA 94305, USA
[3]Department of Chemistry, Stanford University, Stanford, CA 94305, USA
[4]Present address: Molecular and Cell Biology Laboratory, Salk Institute for Biological Studies, La Jolla, CA 92037, USA
*Correspondence: ucho@alumni.stanford.edu (U.C.), jameschen@stanford.edu (J.K.C.)
https://doi.org/10.1016/j.chembiol.2020.07.009

The unique photophysical properties of lanthanides, such as europium, terbium, and ytterbium, make them versatile molecular probes of biological systems. In particular, their long-lived photoluminescence, narrow bandwidth emissions, and large Stokes shifts enable experiments that are infeasible with organic fluorophores and fluorescent proteins. The ability of these metal ions to undergo luminescence resonance energy transfer, and photon upconversion further expands the capabilities of lanthanide probes. In this review, we describe recent advances in the design of lanthanide luminophores and their application in biological research. We also summarize the latest detection systems that have been developed to fully exploit the optical properties of lanthanide luminophores. We conclude with a discussion of remaining challenges and new frontiers in lanthanide technologies. The unprecedented levels of sensitivity and multiplexing afforded by rare-earth elements illustrate how chemistry can enable new approaches in biology.

## INTRODUCTION

Biology is becoming an increasingly molecular and quantitative science, driven by our curiosity about the machinery within cells and organisms. Technological advances have opened new windows into these complex processes, particularly methods that enable the observation of specific molecular structures, interactions, and reactions. A wide-ranging palette of synthetic and genetically encoded fluorophores have been designed (Rodriguez et al., 2017; Wang et al., 2019), and new modalities for photometry, flow cytometry, microscopy, and macroscale imaging have been developed (Feuchtinger et al., 2016; Power and Huisken, 2017; Sigal et al., 2018; Spitzer and Nolan, 2016; Wang and Yao, 2016). In combination, these advances have made possible the detection of transcripts, proteins, metabolites, and other molecules in diverse biological systems.

Despite this significant progress, major technical challenges continue to constrain our ability to visualize biology at the molecular level. For example, biological autofluorescence can preclude the detection of targeted transcripts or proteins at their physiological concentrations. While probes for these macromolecules can be used in conjunction with signal-amplifying technologies, these approaches typically require sample fixation and cannot be used to study living systems (Ali et al., 2014; Bi et al., 2017; Pichon et al., 2018). Commonly used fluorophores also are not optimal for macroscale imaging, as their excitation and emission wavelengths are readily absorbed or scattered by biological tissues.

Our ability to observe the molecular interactions and reactions that create living systems has been similarly constrained. Although fluorescence resonance energy transfer (FRET)-based sensors have been developed for a variety of intermolecular complexes, protein modifications, and metabolic products, their sensitivity and accuracy are limited by their broad excitation and emission bands and modest Stokes shifts (Algar et al., 2019; Bajar et al., 2016; Hochreiter et al., 2015). Achieving a systems-level understanding of biology also requires the simultaneous observation of multiple targets. However, multi-color detection is typically restricted to five or six spectral channels, even with state-of-the-art probes, lasers, and optical filters.

Our efforts to overcome these hurdles would benefit from new chemistries and detection modalities, and lanthanide-based technologies have shown particular promise. Lanthanide complexes and nanoparticles can have unique photophysical qualities, including millisecond scale luminescence lifetimes, large Stokes shifts, ultrasharp emissions, and the ability to undergo resonance energy transfer or photon upconversion. Lanthanide-based probes therefore can be adopted to achieve unparalleled detection sensitivity, multiplexing capacity, and imaging depth, allowing biological systems to be interrogated in novel ways. Yet lanthanide luminophores are not widely utilized for biological imaging. In comparison with conventional fluorophores and fluorescent proteins, lanthanide probes have been limited by their brightness, dependence on UV excitation, and low photon efflux. Recent progress in probe design, instrumentation, and imaging modalities have overcome many of these constraints, sparking renewed interest in these rare-earth metals.

This review focuses on the technological advances that have unlocked the potential of lanthanide luminophores as biological probes. We first describe the photophysics and chemotypes of lanthanide-based probes, comparing their attributes with those of other photoluminescent molecules. We then provide specific examples of how these luminescent metal ions have been applied in photometric assays, biological microscopy, and whole-body imaging. We conclude by discussing

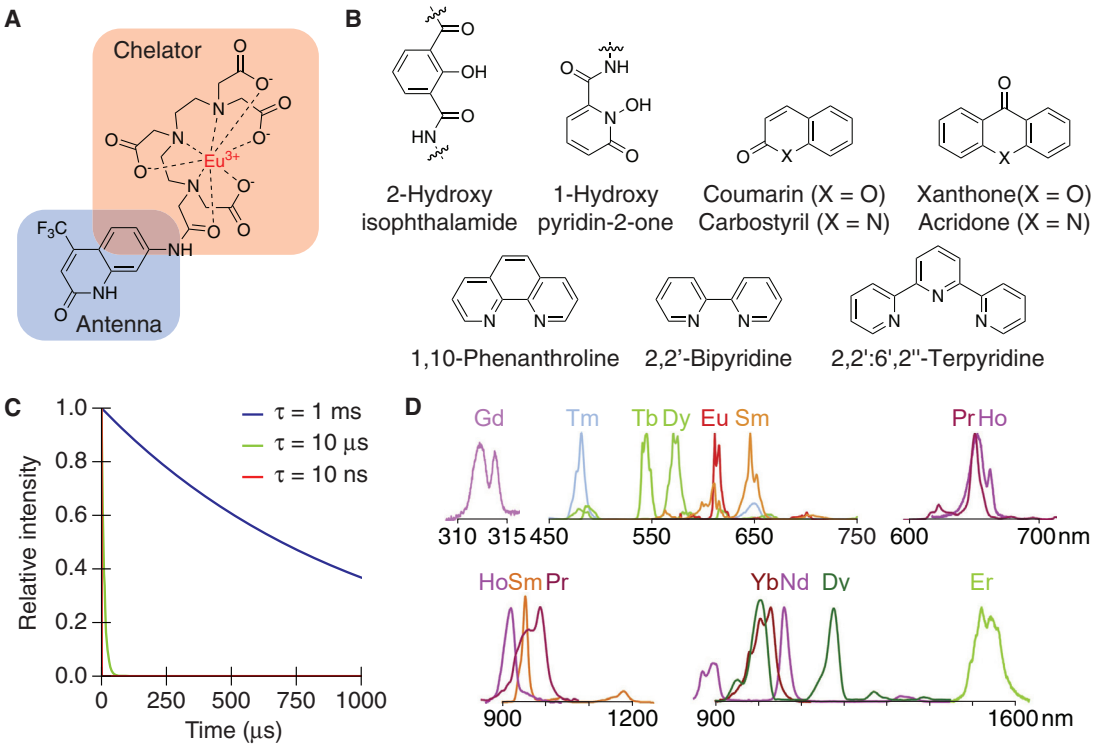


**Figure 1. Photophysical Properties and Chemical Structures of Luminescent Lanthanide Complexes**
(A) Chemical structure of $Eu^{3+}$-DTPA-cs124-$CF_3$ complex, highlighting the chelate and antenna moieties.
(B) Commonly used chromophores in lanthanide chelates.
(C) Theoretical decay curves of luminophores with 10-ns (red), 10-μs (green), and 1-ms (blue) lifetimes.
(D) Emission spectra of trivalent lanthanide ions. Adapted with permission from (Bünzli, 2016).

how lanthanide technologies could be further enhanced to create new opportunities for biological discovery.

## CHEMISTRY OF LANTHANIDE PROBES

### Lanthanide Photoluminescence

Lanthanide luminescence is fundamentally different from fluorescence. The latter is generated when a molecule transitions from one electronic state to the other, whereas lanthanide metal ions luminesce from a parity-forbidden transition within 4*f* atomic orbitals. This distinct photophysical process confers to lanthanides their characteristic spectral properties.

First, the 4*f*-4*f* transitions in luminescent lanthanide ions are "disallowed" by the Laporte selection rule, and their low probabilities result in extinction coefficients that are several orders of magnitude lower than those of commonly used fluorophores (<10 $M^{-1}$ $cm^{-1}$versus 10,000 to 100,000 $M^{-1}$ $cm^{-1}$). Since efficient, direct excitation of these rare-earth metals requires light intensities that are destructive to biological samples, "antenna" chromophores are typically used to transfer energy to lanthanide ions (Figure 1A). Most of these chromophores absorb 300- to 400-nm light and have extinction coefficients that are greater than 10,000 $M^{-1}$ $cm^{-1}$ (Figure 1B; Tables S1 and S2) (Armelao et al., 2010; Heffern et al., 2014; Mathis and Bazin, 2010), and a few that respond to visible light have been developed also (Ma et al., 2018; Tian et al., 2014). The resulting photoluminescence is also associated with Stokes shifts that are several hundred nanometers, allowing clear separation of excitation and emission signals. Moreover, lanthanide probes are resistant to photobleaching since the metal ion serves as a triplet state quencher for the antenna chromophore (Xiao et al., 2011).

Another consequence of the disallowed 4*f*-4*f* transitions is the slow decay of lanthanide excited states, which translates into exceptionally long emission lifetimes. While small organic fluorophores and fluorescent proteins emit light for only several nanoseconds, lanthanide luminescence can last for a few milliseconds (Figure 1C). For example, the luminescence lifetimes of commonly used $Tb^{3+}$ and $Eu^{3+}$ complexes range from 0.5 to 2.5 ms (Nishioka et al., 2006; Xiao and Selvin, 2001; Xu et al., 2011). Since the excited 4*f* states are shielded by the filled $5s^2$ and $5p^6$ subshells, lanthanide luminescence is also highly insensitive to the chemical environment. Lanthanide emissions therefore have very narrow bandwidths (Figure 1D), and individual peaks that originate from different transitions are easily distinguishable. For example, the $Tb^{3+}$ luminescence is characterized by line-like emissions at 490, 540, and 580 nm, and $Eu^{3+}$ luminescence at 590, 610, and 720 nm. Several other lanthanides have ultrasharp emission peaks in the visible range, but their modest quantum yields (<10%) have limited their utility as imaging probes (Moore et al., 2009).

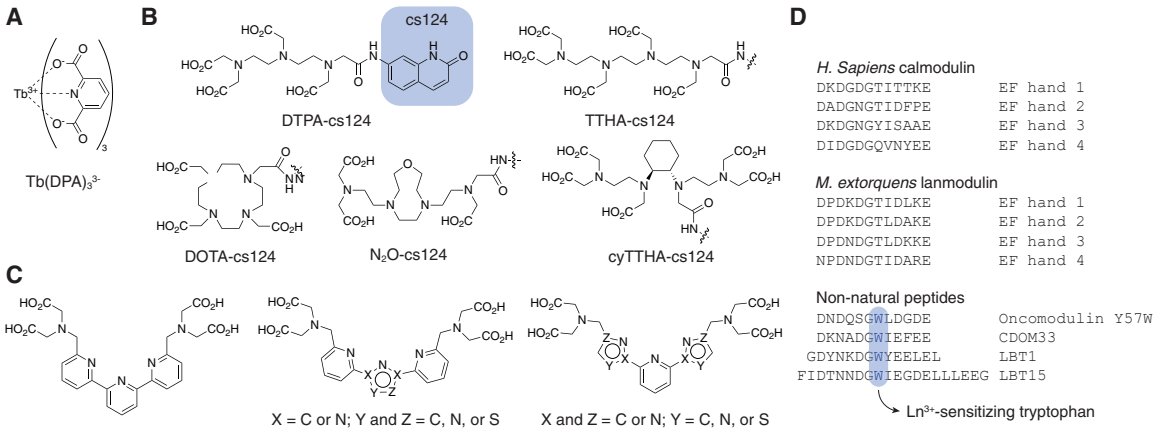


**Figure 2. Lanthanide-Binding Chelates and Peptides**
(A) Chemical structure of $Tb(DPA)_3^{3-}$.
(B) Lanthanide ligands with a polyaminocarboxylate backbone and a cs124 antenna.
(C) Ligands with a terpyridine or terpyridine-like backbone.
(D) Amino acid sequences of lanthanide ion-binding peptides.

## Synthetic Lanthanide Chelates

Chemists have elucidated many of the chemical prerequisites for making bright lanthanide complexes for biological applications. The antenna effect was discovered very early in the study of lanthanide luminescence, and the ability of EDTA and NTA (nitrilotriacetate) chelates to suppress aqueous quenching was described several decades ago (Horrocks et al., 1977; Weissman, 1942). One of the first photoluminescent lanthanide chelates was $Tb(DPA)_3^{3-}$ ([DPA] dipicolinic acid) (Barela and Sherry, 1976) (Figure 2A), and subsequent efforts to develop new lanthanide-based optical probes have strived to maximize molar absorptivity, antenna-to-lanthanide transfer efficiency, quantum yield, photostability, and *in vivo* stability . For example, the Raymond group has developed minimal chromophoric chelators that are optimized for $Tb^{3+}$ and $Eu^{3+}$: IAM (2-hydroxyisophthalamide) and 1,2-HOPO (1-hydroxypyridin-2-one) (Figure 1B) (Moore et al., 2009). These compounds are direct descendants of DPA; both IAM and 1,2-HOPO are bidentate ligands, and four units of IAM or 1,2-HOPO are combined to generate an octadentate complex. In particular, a $Tb^{3+}$ cryptate that contains four IAM molecules, $Tb^{3+}$-Lumi4, is one of the brightest and most long-lived $Tb^{3+}$ complexes (Xu et al., 2011), with an extinction coefficient, quantum yield, and luminescence lifetime of 23,700 $M^{-1}$ $cm^{-1}$, 50%, and 2.45 ms, respectively.

Polyaminocarboxylates functionalized with a single antenna are among the most frequently used lanthanide chelates. The Selvin and Parker groups have synthesized and characterized several probes in this structural class, including DTPA, TTHA, DOTA, and $N_2O$ ligands that are functionalized with carbostyril-based antennae (Ge and Selvin, 2008; Li and Selvin, 1995; Montgomery et al., 2009; Parker and Williams, 1996; Xiao and Selvin, 2001) (Figure 2B; Table S1). In particular, the cs124 chromophore has been coupled with both $Tb^{3+}$ and $Eu^{3+}$, and cs124-$CF_3$ preferentially transfers energy to $Eu^{3+}$, with an extinction coefficient of 15,000 $M^{-1}$ $cm^{-1}$ at 360 nm. Lanthanide-polyaminocarboxylate complexes have varying biological stabilities *in vivo*, making certain classes more amenable to biological applications. For example, DOTA and $N_2O$ chelators can bind trivalent lanthanide ions in the presence of millimolar nucleoside triphosphates (NTPs and dNTPs), but DTPA and TTHA cannot (Cho et al., 2018; Ge and Selvin, 2008; Hewitt et al., 2017).

Multivalent, unimolecular ligands can also be designed to be intrinsically chromophoric. Terpyridine (Mukkala et al., 1993) and terpyridine-like (Mukkala et al., 1996; Takalo et al., 1997) lanthanide chelates pioneered by the Takalo group are the earliest examples of this class (Figure 2C). In the case of 2,2′:6′,2″-terpyridine-based chelates, three nitrogens of the terpyridine moiety coordinate the central lanthanide ion, together with polycarboxylate arms attached to the 6 and 6″ positions. The terpyridine doubles as a light harvesting center. Among the lanthanide complexes that adopt the terpyridine scaffold, $Eu^{3+}$-ATBTA stands out for its brightness and stability (Nishioka et al., 2006). This lanthanide chelate has a 20,000 $M^{-1}$ $cm^{-1}$ extinction coefficient at 360 nm and a quantum yield of 9.1%, and it remains photoluminescent in phosphate-buffered saline even though the $pK_{sp}$ for $EuPO_4$ is ~25 (Firsching and Brune, 1991). The biochemical stability of $Eu^{3+}$-ATBTA is further demonstrated by its perdurance for days in zebrafish embryos (Cho et al., 2018) and ability to withstand heating to 95°C (Nishioka et al., 2006). Accordingly, structurally related $Tb^{3+}$ and $Eu^{3+}$ complexes have been used as TaqMan probes for quantitative polymerase chain reaction, affording a linear detection range spanning six orders of magnitude when monitored by time-gated photometry (Gueimonde et al., 2004; Nurmi et al., 2000, 2002).

## Lanthanide-Binding Protein Motifs

Trivalent lanthanide ions can also form stable complexes with polypeptides. It had long been known that lanthanides can replace $Ca^{2+}$ in biological systems (Nieboer, 1975), and most peptidic lanthanide-binding motifs are derived from $Ca^{2+}$-binding sites (Figure 2D). For example, the Szabo group showed that $Tb^{3+}$ binds strongly to the 14-amino acid loop in EF hand motifs and that $Tb^{3+}$ excitation is promoted by nearby aromatic residues, especially tryptophan (Hogue et al., 1992). The Imperiali group subsequently used a mutagenesis screen to optimize the EF hand-derived lanthanide-binding motif, developing

peptidic ligand with a dissociation constant ($K_D$) of 220 nM (Franz et al., 2003). Further screening yielded a $Tb^{3+}$-binding peptide with a 19-nM $K_D$ (Martin et al., 2005), and antenna chromophores, such as cs124 and acridone, were introduced as unnatural amino acids (Reynolds et al., 2008). More recently, a naturally occurring lanthanide-binding protein lanmodulin was identified from *Methylobacterium extorquens*. This gene product contains four EF hand-like motifs and binds most of the trivalent lanthanide ions with picomolar affinity (Cotruvo et al., 2018). However, it should be noted that lanmodulin lacks a tryptophan sensitizer and therefore is not suitable for photometric assays or imaging.

Lanthanide-binding protein motifs have been extensively used in X-ray crystallography and NMR studies (Barthelmes et al., 2015, 2017; Martin et al., 2007; Silvaggi et al., 2007; Welch et al., 2003; Wöhnert et al., 2003; Zhuang et al., 2008). Lanthanides bound to these peptidic chelators have electron densities and paramagnetic properties that facilitate the determination of macromolecular structures. However, the application of lanthanide-binding protein motifs in live cells and organisms has been limited. Their affinities for free $Tb^{3+}$ and $Eu^{3+}$ cannot prevent ion sequestration by nucleoside triphosphates (Cho et al., 2018; Ge and Selvin, 2008; Morrison and Cleland, 1983) and inorganic phosphate (Firsching and Brune, 1991). In addition, the ability of trivalent lanthanide ions to precipitate phosphoproteins (Güzel et al., 2012) could significantly impede the delivery of soluble lanthanide ions to genetically encoded chelators in live cells and organisms.

### Nanoparticles

Nanoparticles and metal-organic frameworks represent a third class of photoluminescent lanthanide probes. While biological applications of metal-organic frameworks have been limited (Rocha et al., 2011; Xu et al., 2016; Zhao et al., 2018), lanthanide-containing nanoparticles are increasingly being used for *in vivo* imaging. The size of nanoparticles can restrict certain applications as their diameters range from a few nanometers to several tens of nanometers, but their unmatched molar absorptivity and photostability are advantageous (Wu et al., 2015). Typically, lanthanide ions are embedded in a fluoride-based nanoparticle, such as $NaYF_4$, $NaYbF_4$, $NaLuF_4$, and $CaF_2$, and a variety of crystalline shapes have been developed (e.g., sphere, rod, cube, or polyhedron). The surface of a lanthanide-doped nanoparticle can be modified to enable specific biological applications, such as metabolite sensing and targeted delivery (Bagheri et al., 2016; Gee and Xu, 2018).

The photophysics and chemical preparation of lanthanide nanoparticles have been reviewed elsewhere extensively and will not be discussed further here (Chen et al., 2014b; Dong et al., 2015; Wen et al., 2018; Wu et al., 2015). However, one property that makes lanthanide nanoparticles particularly useful for whole-animal imaging is the ability of certain subtypes to undergo photon upconversion. In this process, two or more photons of low energy are absorbed and converted into a single emission photon of higher energy. In other words, the emission wavelength is shorter than that of excitation light (“anti-Stokes emission”). Upconverting nanoparticles have begun to garner the attention of biomedical scientists for two reasons. First, the probes can be both excited and detected by near-IR photons, enabling high-contrast, high-resolution deep-tissue imaging since light attenuation, autofluorescence, and scattering are minimized. Second, upconversion allows near-IR irradiation to trigger photochemical reactions that would otherwise require UV or visible light. For instance, it can be exploited to site-specifically release caged drugs or generate cytotoxic chemical species (Wu et al., 2015).

Lanthanide dopants in nanoparticles facilitate photon upconversion via several different mechanisms, of which the two most common are excited-state absorption and energy transfer upconversion (Figure 3C) (Chen et al., 2014b; Dong et al., 2015; Wang and Liu, 2009). Excited-state absorption is a process that makes use of a single dopant species. It refers to successive absorption of excitation photons by a lanthanide ion (typically $Nd^{3+}$, $Ho^{3+}$, $Er^{3+}$, and $Tm^{3+}$) that has a ladder-like energy level structure. Successive absorption is promoted by the long lifetime of the intermediate excited state of the lanthanide dopants, and emission occurs from a high-lying excited state. In comparison, energy transfer upconversion utilizes two or more lanthanide species. In this process, excitation energy harvested by a “sensitizer” ion (donor) is passed on to the “activator” ion (acceptor). The transfer can occur twice or more from the same sensitizing ion or from multiple sensitizers to a single activator. $Yb^{3+}$ is the most preferred sensitizer since it has only one excited-state level and absorbs strongly in the 960- to 990-nm window, which can be efficiency targeted by several conventional IR lasers. $Yb^{3+}$ is often coupled with $Ho^{3+}$, $Er^{3+}$, or $Tm^{3+}$ activators, and these acceptor ions generate violet-to-red wavelength photons from IR excitation, depending on the degree of upconversion (Figure 3D).

It is important to note that photon upconversion fundamentally differs from two-photon absorption, a non-linear optical process exploited for two-photon confocal microscopy. The latter requires simultaneous interaction of two photons with a chromophore while the former relies on metastable states between the ground and excited states, which facilitate sequential energy absorption. In comparison, upcoversion is a linear optical process that is orders of magnitude more efficient.

## COMPARISON WITH OTHER PHOTOLUMINESCENT PROBES

### Fluorescent Proteins

Fluorescent proteins have become the work horses of biological imaging due to their genetic encodability and broad color palette. Just as protein engineers have extensively mutagenized fluorescent proteins to optimize their greater brightness and photostability, chemists have developed synthetic lanthanide chelates with photophysical properties that are ideal for biological imaging. The latest lanthanide probes have overall quantum yields ($E_{TRANS}$ x $QY_{Ln}$, Figure 3A) that are comparable with those of red fluorescent proteins, which typically range from 20% to 50% (Piatkevich and Verkhusha, 2011) (Table S2). For example, when $Tb^{3+}$ or $Eu^{3+}$ is complexed with a TTHA chelate functionalized with a cs124 or cs124-$CF_3$ chromophore, the resulting chelate has an overall quantum yield of approximately 40% (Chen and Selvin, 2000b; Xiao and Selvin, 2001).

In addition, the extinction coefficients of lanthanide probes are similar to those of blue and cyan fluorescent proteins (Day and

Davidson, 2009), defined primarily by the antenna moiety (Figure 1B; Table S2). Most antenna chromophores are aromatic polycycles, and widely used $Tb^{3+}$ and $Eu^{3+}$ sensitizers include bipyridines, 1,10-phenanthroline, terpyridines, tetraazatriphenylene, coumarins, xanthones, and acridones (Armelao et al., 2010; Heffern et al., 2014; Mathis and Bazin, 2010). Appending a single chromophore to the core chelate scaffold can achieve molar absorptivities of 10,000–50,000 $M^{-1}$ $cm^{-1}$.

While fluorescent proteins can be appended to a protein of interest by genetic fusion, lanthanide complexes require a chemical handle for *in vivo* protein tagging. For example, trimethoprim-, $O^6$-benzylguanine-, or $O^2$-benzylcytosine-functionalized lanthanide complexes have been used to label dihydrofolate reductate-, SNAP-, or CLIP-fused proteins (Emami-Nemini et al., 2013; Faklaris et al., 2015; Levoye et al., 2015; Pou et al., 2012; Rajapakse et al., 2010). For *in vitro* labeling of macromolecules, such as antibodies, streptavidin, and oligonucleotides, standard coupling methods can be used. Azide (Pillai et al., 2012), isothiocyanate (Li and Selvin, 1997; Takalo et al., 1997), maleimide (Ge and Selvin, 2004), and cyanuric chloride (Mukkala et al., 1993, 1996; Nishioka et al., 2006) moieties have been utilized for the bioconjugation of lanthanide chelates.

### Other Long-Lived Photoluminescent Reagents

The defining feature of lanthanide luminescence is its long lifetime, which is $10^5$- to $10^6$-fold greater than that of conventional fluorescence. Other luminophores with emission lifetimes that exceed tens of nanoseconds include organic compounds that emit delayed fluorescence or room temperature phosphorescence, transition-metal complexes, and quantum dots.

Organic compounds can generate >10-ns photoluminescence via three different mechanisms: (1) n-to-$\pi^*$ excitation, (2) excimer formation, and (3) structural suppression of $T_1$-to-$S_0$ nonradiative decay pathways. Several organic molecules that exploit these photophysical processes have been reported (Maltman et al., 2010; Nau and Zhang, 1999; Patsenker et al., 2011; Rich et al., 2013; Smith et al., 2004; Wawrzinek et al., 2013), but in general they make poor biological probes. n-to-$\pi^*$ fluorophores have low extinction coefficients as the transition is parity forbidden. Small molecules that form excimers have extended, highly conjugated ring systems, which decrease water solubility and increase non-specific binding in biological systems. Room temperature phosphorescence requires a binding cavity in a protein, cyclodextran, or polymeric matrix to minimize the nonradiative inactivation of $T_1$ states. For these reasons, their usage in biomedical imaging has been restricted.

Phosphorescence from transition-metal complexes (e.g., $Re^+$, $Ru^{2+}$, $Os^{2+}$, $Ir^{3+}$, $Rh^{3+}$, $Pt^{2+}$, $Au^+$, and $Cu^+$) have much in common with lanthanide-based luminescence: long Stokes shifts, microsecond to millisecond scale emission lifetimes, and sharp emissions (Baggaley et al., 2014; Lo et al., 2012; Yam and Wong, 2011). However, transition-metal phosphorescence stems from a totally disparate electronic process, namely ligand-to-metal or metal-to-ligand charge transfer. Like organic phosphors, these heavy-metal complexes are sensitive to oxygen and solvent polarity, making them versatile sensors but poor tags for visualizing proteins or oligonucleotides. In addition, they typically carry multiple polypyridine ligands (2,2′-bipyridine, terpyridine, or 1,10-phenanthroline), which results in low water solubility and high cytotoxicity.

Quantum dots can be engineered to have long emission lifetimes by changing their size (Chen et al., 2014a; Zhang et al., 2016) or doping these nanoparticles with transition metals (e.g., $Mn^{2+}$, $Cu^{2+}$, or $Ni^2$) or trivalent lanthanide ions (e.g., $Tb^{3+}$, $Eu^{3+}$, $Er^{3+}$, $Tm^{3+}$, $Ho^{3+}$, or $Yb^{3+}$) (Chen et al., 2015; Wu and Yan, 2013; Zhang et al., 2017). The former strategy can extend the emission lifetime of a quantum dot to a few hundreds of nanoseconds at best, whereas the latter approach enables microsecond to millisecond scale delayed photoluminescence. More recently, silicon-based quantum dots with emission lifetimes in the double-digit μs range have been developed (Tu et al., 2016; Yang et al., 2019), but their large size (>100 nm) is prohibitive for many biological applications.

### Luminescence Resonance Energy Transfer

Lanthanide luminophores can participate in an energy transfer process analogous to FRET, which is referred to as luminescence resonance energy transfer (LRET) (Figure 3A). Common synthetic fluorophores and fluorescent proteins have been successfully adopted as LRET acceptor molecules, including cyanine, Atto, and Alexa Fluor dyes (Geissler et al., 2013), eGFP (Rajapakse et al., 2010), TagRFP (Bhattacharya et al., 2018), mCherry (Kubota et al., 2014), and allophycocyanin (Mathis, 1993). The Hildebrandt group and others have demonstrated that even quantum dots can be LRET acceptors (Charbonniere et al., 2006; Cui and Parker, 2016; Geissler et al., 2010; Hildebrandt et al., 2005).

LRET has several unique advantages over FRET. The Förster radius of a donor-acceptor pair ($R_0$, the distance at which energy transfer is 50% efficient) is proportional to (1) the one-sixth power of the overlap integral of the donor emission and acceptor absorbance ($J^{1/6}$) and (2) the one-sixth power of the donor quantum yield ($QY^{1/6}$). Lanthanide-based donors have a comparative advantage over their fluorescent counterparts in both areas. Due to their line-like emission peaks, lanthanide probes achieve J values that are about an order of magnitude greater than those of fluorescent donors (George Abraham et al., 2015). The quantum yield of a $Tb^{3+}$ complex can exceed 70% while those of fluorescent proteins that emit in a similar spectral window (e.g., eYFP, Venus, mKO2, and mOrange) are 60%–70% (Day and Davidson, 2009). Similarly, the quantum yield of a $Eu^{3+}$ complex can be as high as 43%, and those of the spectrally matched mCherry, mRuby, and mKate2 proteins are 20%–40% (Day and Davidson, 2009). These attributes enable LRET donor-acceptor pairs to have larger $R_0$ distances than their FRET counterparts; LRET $R_0$ values range from 5 to 10 nm, whereas FRET $R_0$ values are typically between 1.5 and 7 nm (Bajar et al., 2016; Müller et al., 2013).

$R_0$ values are also influenced by the relative orientations of the donor and acceptor transition dipole moments ($\kappa^2$), which can range from 0 to 4. $\kappa^2$ is usually assumed to be 2/3, which occurs when the resonance energy transfer pair achieves complete rotational diffusion during the donor lifetime. Since the molecular tumbling and donor decay timescales are both in the low-nanosecond regime (Gáspári and Perczel, 2010; Ortega et al., 2013), this assumption is often invalid for FRET. In contrast, lanthanide donors can remain in their excited states for a few milliseconds,

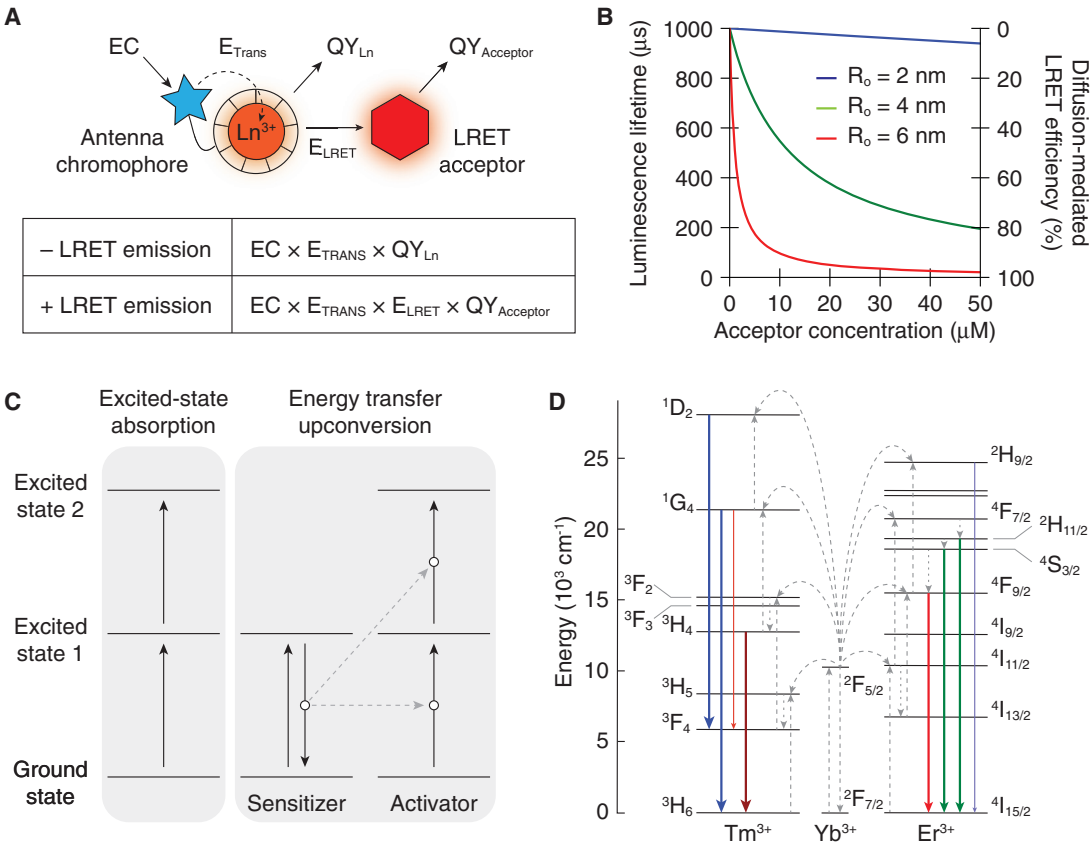


**Figure 3. Luminescence Resonance Energy Transfer**

(A) Energy transitions involved in direct lanthanide and LRET emissions. EC, extinction coefficient; $E_{TRANS}$, antenna-to-lanthanide transfer efficiency; $E_{LRET}$, LRET efficiency; and QY, quantum yield. $E_{LRET}$ is equal to $1 - \tau_{+LRET}/\tau_{-LRET}$.

(B) Concentration- and $R_0$-dependent effects of an LRET acceptor on lanthanide luminescence. (donor emission lifetime of 1 ms and distance of closest approach of 0.5 nm).

(C) Energy transitions of excited-state absorption and energy transfer upconversion. Energy transfer steps are indicated by the dashed arrows.

(D) Energy levels of $Tm^{3+}$, $Yb^{3+}$, and $Er^{3+}$, and potential energy transfer upconversion pathways. Adapted with permission from Wang and Liu (2009).

providing sufficient time for both the donor and acceptor to rotationally diffuse and yielding a $\kappa^2$ value very close to 2/3 (Selvin, 1996). The minimal $R_0$ stochasticity associated with LRET allows donor-acceptor distances to be determined with greater accuracy than FRET-based methods.

Finally, lanthanide donors enable "diffusion-mediated" resonance energy transfer. This process depends not only on $R_0$ but also on the diffusion coefficients of the donor and acceptor molecules, the acceptor concentration, and the distance of closest approach for the donor-acceptor pair. Since lanthanide luminophores are long-lived, they can approach within one Förster radius of an LRET acceptor during their excited state (Thomas et al., 1978). The diffusion rates of small metal complexes and organic fluorophores are typically in the $10^{-5}$ to $10^{-6}$ $cm^2$ $s^{-1}$ range (Furukawa et al., 2007; Nitsche et al., 2004), and near-unity LRET efficiency is therefore predicted to occur when acceptor concentrations are in the low micromolar range and $R_0$ is greater than 6 nm (Figure 3B). This has been experimentally confirmed with $Tb(DPA)_3^{3-}$/rhodamine B (Thomas et al., 1978) and $Eu^{3+}$/ATBTA/Atto 610 (Cho et al., 2018). When lanthanide donors are paired with fluorescent proteins for diffusion-mediated LRET, high acceptor concentrations are required since the β barrel scaffold blocks close access to the genetically encoded fluorophore.

## Multiplexing Capabilities

The long photoluminescence lifetimes, narrow emission bands, long Stokes shifts, and LRET capabilities of lanthanide chelates also make these probes ideal for multiplexing. Spectrally distinct lanthanide complexes can be used in combination, achieving a multiplexing capacity that far exceeds that of conventional fluorophores. Two different strategies have been pursued: one approach makes use of temporal multiplexing (in combination with spectral multiplexing), while the other uses mixtures of lanthanides at predetermined ratios, taking advantage of their ultrasharp emission peaks.

Multiplexing through temporal gating was first demonstrated by the Selvin group (Chen and Selvin, 2000a) (Figure 4A). They labeled the 5′ ends of DNA oligonucleotides with either $Tb^{3+}$-DTPA-cs124 or fluorescein and generated duplexes containing 6, 8, or 10 base pairs. Due to their varying LRET efficiencies, the labeled duplexes had luminescence lifetimes of 62, 266, and 540 μs, respectively. In addition, a 10-base pair duplex with $Eu^{3+}$-DTPA-cs124 and Cy5 labels exhibited an emission

lifetime of 250 μs. Their work established a means of kinetically identifying specific double-stranded DNA structures. In principle, the number of resolvable targets can be quadratically increased by integrating both time and wavelength domains.

A similar concept was recently realized by the Jin group using two different lanthanide materials. They encapsulated in porous polystyrene beads a fixed amount of $Eu^{3+}$-(thenoyltrifluoroacetonate)$_3$ and a varying amount of red-adsorbing coumarin LRET acceptor (Lu et al., 2014a), creating a dozen types of lifetime-encoded microspheres (Figure 4B; $\tau$ = 188–359 μs). The Jin group also developed "τ-dots" with varying photon upconversion efficiencies and therefore unique lifetime codes (Lu et al., 2014b). These NaYF4:$Yb^{3+}$ nanoparticles were doped with differing concentrations of $Tm^{3+}$ activator ion to achieve emission lifetimes ranging from 26 to 662 μs, enabling the generation of images with multiple lifetime encoded layers.

The Fordyce group has pushed the limits of lanthanide probe multiplexing (Gerver et al., 2012; Nguyen et al., 2017) (Figure 4C). Using $Eu^{3+}$, $Dy^{3+}$, and $Sm^{3+}$ nanoparticles, they synthesized polymeric beads that contain predetermined ratios of $Dy^{3+}$:$Eu^{3+}$ and $Sm^{3+}$:$Eu^{3+}$. The resulting 24 spectrally encoded microspheres were successfully distinguished by linear unmixing using six reference spectra. The group has since increased the library size to 550 barcodes by adding $Ce^{3+}$/$Tb^{3+}$ and $Tm^{3+}$ nanoparticles to the combinations. This technology, termed MRBLE (microspheres with ratiometric barcode lanthanide encoding), has been used to screen a peptide library for calcineurin ligands (Nguyen et al., 2019), and the Cyert group used the resulting leads to search *in silico* for potential calcineurin substrates in the human proteome (Wigington et al., 2019). Of 691 candidate proteins, 45 novel calcineurin targets have been experimentally confirmed, including several nuclear pore complex and centrosomal proteins.

## BIOLOGICAL APPLICATIONS OF LANTHANIDE PROBES

### Photometric Assays

Lanthanide luminophores first emerged as an alternative to radioisotopic labels in immunoassays. Using a first-generation, temporally gated photometer (Figure 5A), the Soini group demonstrated that a 400-μs delay between the sample excitation and detection allowed the selective collection of photons emitted from a $Eu^{3+}$ complex (Soini and Kojola, 1983). Background autofluorescence was completely suppressed, and the detection sensitivity of their system matched that of $^{125}$I-based radiography. Ultrasensitive photometric assays remain the most common application of lanthanide probes in the biosciences.

DELFIA (dissociation-enhanced lanthanide fluorescence immunoassay) developed by the Hemmilä group is another popular technique that takes advantage of lanthanide emission lifetimes (Dickson et al., 1995; Hemmilä, 1985, 1988; Hemmilä et al., 1984; Ogata et al., 1992) (Figure 5B). This method is a variant of the enzyme-linked immunosorbent assay, in which a secondary antibody is tagged with a $Eu^{3+}$ complex rather than a signal-amplifying enzyme, such as horseradish peroxidase. After washing, $Eu^{3+}$ ions are released from the antibody-chelate conjugates by acidification, and luminescence "enhancers," such as 2-naphthoyltrifluoroacetone and trioctylphosphine oxide, are then added for the time-gated detection of $Eu^{3+}$ luminescence. DELFIA achieves attomolar detection sensitivity and its compatibility with several trivalent lanthanide ions allows multiplexing. The technique has been primarily used to quantify hormones and cytokines in human blood samples, with a fg/mL detection limit (Zhang et al., 2014b). The sensitivity of DELFIA can be further enhanced by orders of magnitude by using $Eu^{3+}$ nanoparticles that can each release thousands of metal ions at low pH (Zhou et al., 2014). This approach has been used to detect carcinoembryonic antigen protein, a colorectal cancer marker.

Time-resolved LRET assays are another exciting example that demonstrates the experimental capabilities enabled by lanthanide-based probes (Bhattacharya et al., 2018; Cha et al., 1999; Emami-Nemini et al., 2013; Faklaris et al., 2015; Gonzalez et al., 2008; Kubota et al., 2017; Mathis, 1995). For instance, LRET is an attractive alternative to FRET for probing protein conformations. In both cases, the protein of interest is typically labeled at two different sites, one with a donor and the other with an acceptor luminophore, and their distance from each other can be determined by the donor-acceptor energy transfer efficiency. FRET measurements are limited by (1) the overlap between the donor and acceptor spectra and (2) donor-only or acceptor-only species that can arise from incomplete bioconjugation. However, LRET emissions can be detected exclusively by combining spectral and temporal filtering (Chen and Selvin, 2000a; Cho et al., 2018; Selvin and Hearst, 1994; Selvin et al., 1994; Vereb et al., 1998; Xiao and Selvin, 2001). Furthermore, the luminescence lifetime of the LRET emission can be directly converted to LRET efficiency ($E_{LRET} = 1 - \tau_{sensitized}/\tau_{donor\text{-}only}$). For example, the Selvin and Bezanilla groups structurally characterized the *Shaker* potassium channel by modifying individual subunits with either $Tb^{3+}$-DTPA-cs124 or fluorescein and monitoring the resulting LRET signals (Cha et al., 1999). The *Shaker* pore has 4-fold rotational symmetry, and by fitting the LRET emission decay to a biexponential curve, they were able to measure inter-subunit distances and detect voltage-dependent changes in pore structure. A similar approach was used to investigate the actin-dependent conformational change of smooth muscle myosin protein (Xiao et al., 2003), demonstrating that the myosin lever arm swings only in the presence of both actin and ADP (Whittaker et al., 1995)

The ability of lanthanide chelates to undergo diffusion-mediated LRET has also been exploited to study protein function. For instance, the Durroux and Bachelerie groups developed an LRET-based photometric assay for quantifying ligand-induced internalization of G protein-coupled receptors (GPCRs), a process that regulates the de- and re-sensitization of these signaling proteins (Levoye et al., 2015) (Figure 5C). In this system, an SNAP tag is genetically fused to an extracellular region of the GPCR of interest and then covalently labeled with cell-impermeable $Tb^{3+}$-Lumi4-$O^6$-benzylguanine. GPCR ligands are then co-administered with fluorescein as a soluble LRET acceptor. Diffusion-mediated LRET between surface-localized GPCRs and the extracellular fluorescein gives rise to long-lived luminescence signals; however, once internalized, $Tb^{3+}$ complex-labeled GPCRs cannot participate in this process. Thus, time-gated measurements of $Tb^{3+}$-Lumi4 and fluorescein signals could be used to determine the degree of GPCR

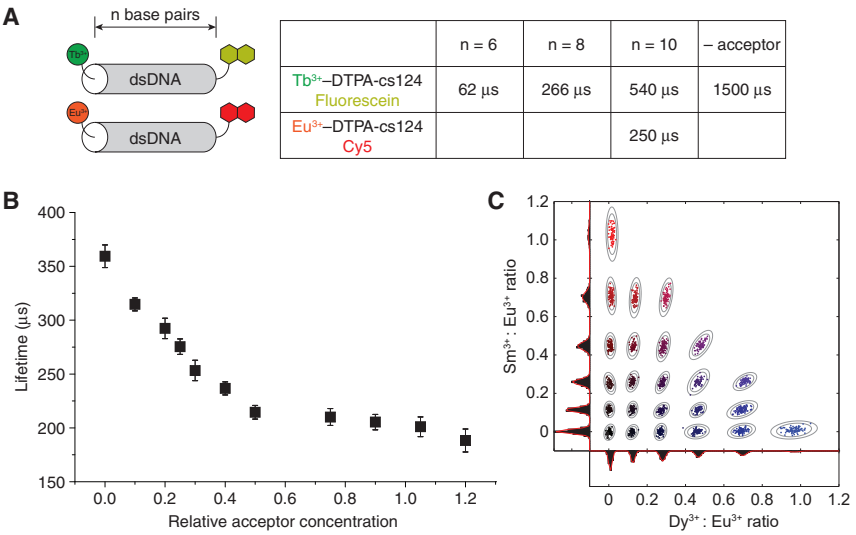


| | n = 6 | n = 8 | n = 10 | – acceptor |
|---|---|---|---|---|
| $Tb^{3+}$–DTPA-cs124 Fluorescein | 62 μs | 266 μs | 540 μs | 1500 μs |
| $Eu^{3+}$–DTPA-cs124 Cy5 | | | 250 μs | |

**Figure 4. Multiplexing Using Lanthanide Luminophores**
(A) Length-dependent LRET emission lifetimes for DNA duplexes functionalized with a lanthanide chelate and acceptor chromophore.
(B) Emission lifetimes of microspheres containing a fixed amount of lanthanide chelate and variable acceptor loading. Adapted from Lu et al. (2014a) under a Creative Commons license.
(C) Lanthanide nanoparticles can be optically differentiated by adjusting the ratios of three trivalent ions ($Sm^{3+}$, $Eu^{3+}$, and $Dy^{3+}$). A scatterplot of the $Dy^{3+}/Eu^{3+}$ and $Sm^{3+}/Eu^{3+}$ luminescence ratios for 1,926 beads with 24 distinct spectral codes is shown. Adapted with permission from Gerver et al. (2012).

internalization in response to various ligands. Diffusion-mediated LRET also has been used to determine the transmembrane depth of bacteriorhodopsin-bound retinal (Leder et al., 1989) and to quantify the lateral diffusion of membrane proteins (Lan et al., 2015).

## Microscopy

Time-resolved luminescence microscopy uses the same detection principles as the photometric assays described above (Figure 5A). First-generation microscopes for time-resolved lanthanide imaging relied on xenon flashlamps for pulsed excitation, and temporal gating was achieved with mechanical chopper blades (Beverloo et al., 1990; Marriott et al., 1994; Seveus et al., 1992), a cost-effective approach that is still used today (Jin and Piper, 2011; Zhang et al., 2014a). For example, the Jin group successful imaged $Eu^{3+}$-labeled *Giardia lamblia* cysts and *Cryptosporidium parvum* oocysts in aqueous media with significant amounts of fluorescent background. A 5-μs delay between sample excitation and emission acquisition completely removed autofluorescence signals and allowed visualization of long-lived lanthanide luminescence within the microorganisms. Chopper-based microscopes also have been used to image lanthanide luminophores in *Daphnia magna*, *Caenorhabditis elegans*, and *Danio rerio* (Ma et al., 2017, 2018; Song et al., 2015; Zhu et al., 2016).

Other groups have built time-resolved microscopes with intensified charge-coupled device (ICCD) cameras that allow electronical time gating and obviate the need of mechanical choppers (Beeby et al., 2000; Cho et al., 2018; Hanaoka et al., 2007; Rajapakse et al., 2010). For example, the Miller group used this system and a UV LED to visualize interactions between ZO-1 and Claudin-1, proteins that are involved in the formation of tight junctions between cells. The two proteins were fused to dihydrofolate reductase and GFP, respectively, and the former was labeled with trimethoprim-functionalized $Tb^{3+}$-Lumi4. ZO-1/Claudin-1 binding was then confirmed by LRET between $Tb^{3+}$-Lumi4 and GFP. In addition to xenon flashlamps and LEDs, pulsed lasers have been adopted as a light source for time-resolved lanthanide microscopy (Afsari et al., 2016; Beeby et al., 2000; Chen et al., 2018; Cho et al., 2018). For example, the Huang and Hildebrandt groups modified the surfaces of 6- and 12-nm quantum dots with either a $Eu^{3+}$ or $Tb^{3+}$ complex, generating LRET pairs with distinct emission lifetimes (Chen et al., 2018). The nanoparticles were used to label four different populations of HeLa cells, which were then mixed and imaged with a time-resolved microscope equipped with an ICCD camera and 349-nm pulsed laser. The differentially labeled HeLa cell populations could be readily discerned by their luminescence lifetimes and, in theory, the multiplexing capacity of this system could be increased by severalfold using quantum dots that emit at different wavelengths.

These advances in time-resolved microscopy have also fostered the development of lanthanide-based sensors for biological imaging. Chemosensors for cations, anions, pH, and metabolites have been developed steadily since the 1990s, but their applications were restricted to photometric assays until the 2010s. The two most common approaches for designing lanthanide chemosensors are to modulate lanthanide ion hydration or antenna activity (Aulsebrook et al., 2018; Shuvaev et al., 2017) (Figure 5D). The Yuan group has shown that these probes can be used in conjunction with time-resolved luminescence microscopy to detect various biomolecules in cells and small organisms, such as *Daphnia magna*, *Caenorhabditis elegans*, and *Danio rerio*. For instance, lanthanide-based probes have been developed to image reactive oxygen species (Ma et al., 2018; Sun et al., 2015; Tang et al., 2019b), nitric oxide (Dai et al., 2017; Tian et al., 2015), hypochlorous acid (Liu et al., 2017; Ma et al., 2017), ascorbic acid (Song et al., 2015), $Zn^{2+}$ (Ye et al., 2014), glutathione (Song et al., 2019), and carbon monoxide (Tang et al., 2019a). Since trivalent lanthanide ions have also been used as magnetic resonance imaging contrast agents (Heffern et al., 2014), certain lanthanide-based sensors could be used for both cell and whole-body imaging. The glutathione sensor, which was used for optical imaging in HeLa cells and zebrafish and for magnetic resonance imaging in mice, exemplifies this paradigm and demonstrates the versatility of lanthanide probes.

Despite their unique photophysical properties, lanthanide chelates are still not widely utilized for biological imaging, primarily

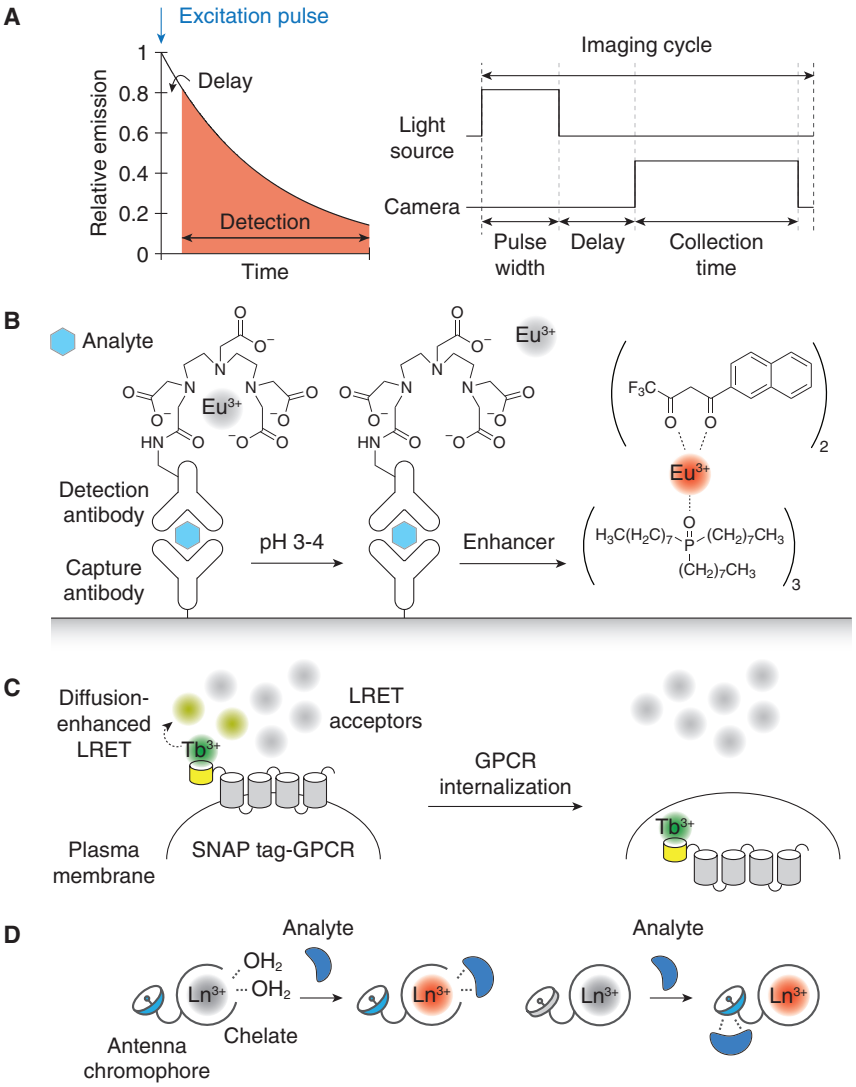


**Figure 5. Lanthanide Luminescence-Based Bioanalytical Techniques**
(A) Time-resolved luminescence detection using pulsatile excitation and temporally gated photon collection.
(B) Schematic representation of DELFIA.
(C) Detection of GPCR internalization by diffusion-enhanced LRET.
(D) Common design principles for lanthanide-based chemosensors.

due to their low photon efflux (Gahlaut and Miller, 2010; Jin et al., 2007a, b; Jin and Piper, 2011; Rajendran and Miller, 2015; Soini et al., 2003). It typically takes ~100,000-fold longer to collect the same number of photons from a lanthanide luminophore than from a fluorophore of the same brightness. Photon efflux is limited further by the pulsatile LED illumination typically used for time-resolved microscopy, which excites <0.1% of the lanthanide probes per pulse (Cho et al., 2018). As a result, time-resolved lanthanide microscopy can require tens of seconds to acquire a single image with sufficient pixel intensities. Lanthanide imaging has also been constrained by the long-lived photoluminescence that is intrinsic to common microscope optics (Cho et al., 2018; Gahlaut and Miller, 2010; Rajendran et al., 2014) (Figure 6A). Although fluorescent emissions can be suppressed by a microsecond scale delay, optics-derived background has lifetimes comparable with that of lanthanide luminescence and thus cannot be efficiently filtered. The undesired photoluminescence originates from UV-excitable materials in objective lenses, and it significantly degrades the sensitivity of lanthanide microcopy. Utilizing high-UV-transmission objectives or narrowband emission filters enhances signal-to-noise ratios by only a few fold (Cho et al., 2018; Rajendran et al., 2014). Together, these factors have prevented lanthanide imaging from recapitulating the detection sensitivities achieved in photometric assays.

We recently overcame these limitations with a new lanthanide imaging modality, trans-reflected illumination (Figure 6B) with LRET (trLRET) (Cho et al., 2018). In trLRET, low lanthanide photon efflux is addressed by using an LRET acceptor that reduces luminescence lifetimes from the millisecond to microsecond regime. Lanthanide-based emission rates increase proportionally with LRET efficiency, permitting imaging cycle rates that are at least 40-fold higher than that of lanthanide donors alone (Figure 6C). Our imaging platform also utilizes a Q-switched laser source rather than an LED, enabling 40% of the lanthanide probes to be excited in a single nanosecond-scale pulse. In combination, these two methods greatly enhance lanthanide photon flux.

To mitigate optics-derived background signals, trLRET uses trans-illumination rather than epi-illumination. This optical configuration allows a $TiO_2$-coated glass insert to be placed in the excitation light path. Since the $TiO_2$ coating attenuates UV light by 100,000-fold, this optical configuration minimizes the excitation of photoluminescent materials in the microscope objectives and can increase the signal-to-noise ratio by 75-fold (Figure 6D). trLRET microscopy has been used to image endogenous proteins in zebrafish embryos with at least an order of magnitude greater sensitivity than standard epifluorescence microscopy (Figure 6E) (Cho et al., 2018). trLRET can also enable the visualization of molecular interactions *in vivo* when the resonance energy transfer is predominantly proximity dependent rather than diffusion mediated (Cho et al., 2018).

## Deep-Tissue Imaging

In addition to cells and embryos, deep tissues can be imaged with photoluminescent lanthanides. One approach utilizes lanthanide-based nanoparticles that are capable of photon upconversion, taking advantage of the paucity of biological molecules that can undergo this photophysical process. Since the

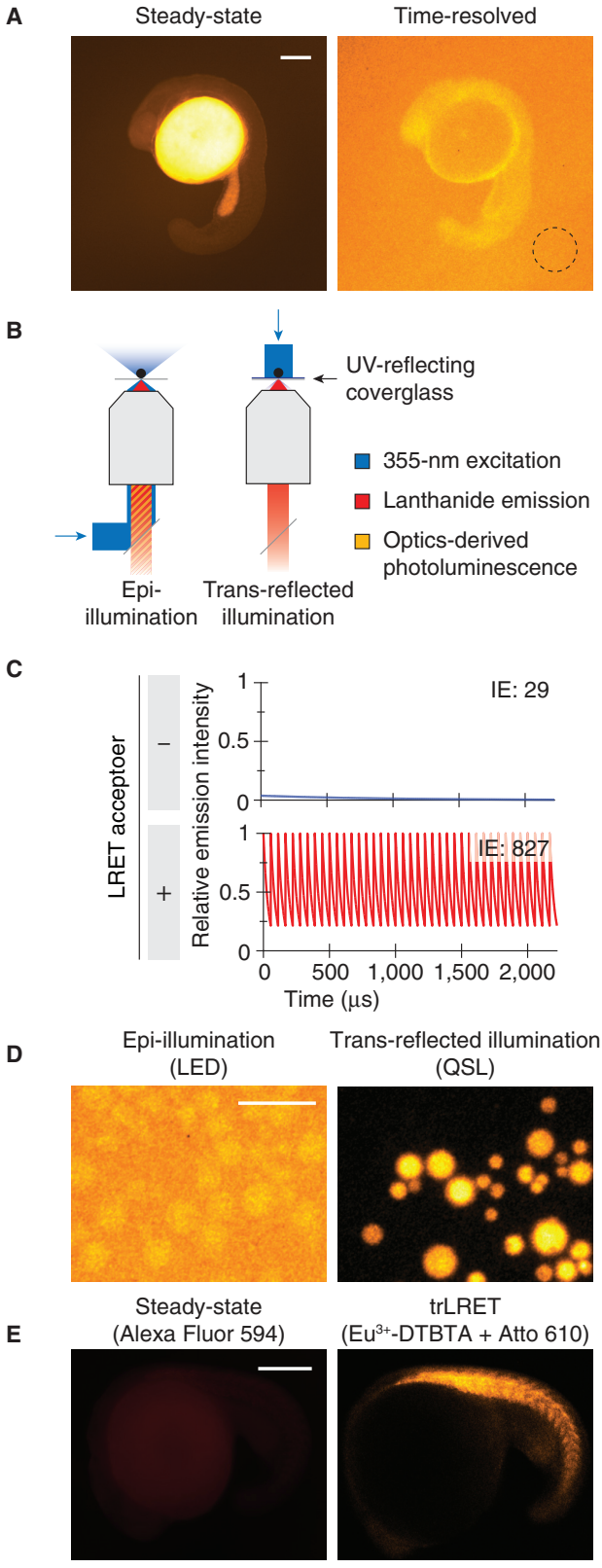


**Figure 6. Time-Resolved Luminescence Microscopy**

(A) Micrographs of zebrafish embryos injected with $Eu^{3+}$-DTBTA-dextran obtained by steady-state and time-resolved microscopy. The optics-derived photoluminescence (e.g., region within the dashed circle) overlaps spectrally and temporally with lanthanide emissions.

(B) Optical paths of epi-illumination (left) and trans-reflected illumination (right) microscopy.

(C) Comparison of conventional and LRET-enhanced time-resolved imaging. The integrated emission intensity (IE) for each condition is shown.

(D) Suppression of optics-derived photoluminescence by trans-reflected illumination.

(E) Comparison of steady-state immunofluorescence and trLRET microscopy, demonstrating the greater detection sensitivity afforded by lanthanide probes. Zebrafish embryos stained with an anti-MYH1E antibody labeled with either Alexa Fluor 594- or $Eu^{3+}$-DTBTA are shown. Scale bars, 200 μm. Adapted with permission from Cho et al. (2018).

upconverted signals have shorter wavelengths than the excitation light, they can be spectral filtered of biological autofluorescence with near-complete efficiency. The Li group showed that nanocrystals doped with $Gd^{3+}$, $Yb^{3+}$, and $Tm^{3+}$ can be imaged in mice with a penetration depth of approximately 2 cm using 980-nm excitation and 800-nm detection (Liu et al., 2011). Similarly, the Prasad and Han groups showed that $Tm^{3+}$-containing nanoparticles can be imaged in mice with negligible background signals (Figure 7A), and the lanthanide probes can even be detected through 3 cm of porcine tissue (Chen et al., 2012).

Lanthanide nanoparticle imaging can be further enhanced by time gating, as their luminescence lifetimes (tens to hundreds of microseconds) are orders of magnitude longer than that of sample autofluorescence. This mode of detection is compatible with both upconverting and downconverting probes. For example, the Jin group showed that a microsecond scale delay facilitates the visualization of $Yb^{3+}$- and $Tm^{3+}$-doped nanoparticles that are subcutaneously injected into mice (Zheng et al., 2016). More recently, the Rodriguez and Chen groups synthesized lanthanide ion-doped $NaGdF_4$ and $NaYF_4$ nanoparticles with long emission lifetimes that can be excited with an 808-nm laser, thereby averting thermal damage to the biological specimen (Tan et al., 2018). The $NaGdF_4$ nanoparticle was orally administered to mice and, immediately after, its presence in the stomach was confirmed by time-resolved imaging (Figure 7B). Furthermore, the $NaYF_4$ nanoparticle was injected into the murine brain and its luminescence could also be detected with high contrast using temporal gating (Figure 7C). These examples illustrate how lanthanide photophysics enables greater contrast and penetration depth for deep-tissue imaging.

Lanthanide-based nanoparticles can also enable deep-tissue imaging with unprecedented levels of spatial resolution. This is achieved by targeting the near-IR-IIb spectrum (1,500–1,700 nm) where light scattering is significantly diminished (Ding et al., 2018). Until very recently, there were only a handful of probes compatible with this optical window (Diao et al., 2015; Zhang et al., 2018), but several $Er^{3+}$-doped nanoparticles with these spectral properties have been developed (Kamimura et al., 2017; Xue et al., 2018; Zhong et al., 2017). The 1,550-nm $Er^{3+}$ emission affords a spatial resolution of a few tens to hundreds of micrometers, which is sufficient to visualize major blood vessels in live mice. Of note, the Piper and Zhang groups have generated $Er^{3+}$-based nanoparticles with varying luminescence lifetimes (microsecond to millisecond) by controlling the energy relay structure (Fan et al., 2018). By conjugating these lifetime-encoded probes to antibodies against surface cancer markers, they were able to simultaneously image multiple antigens on

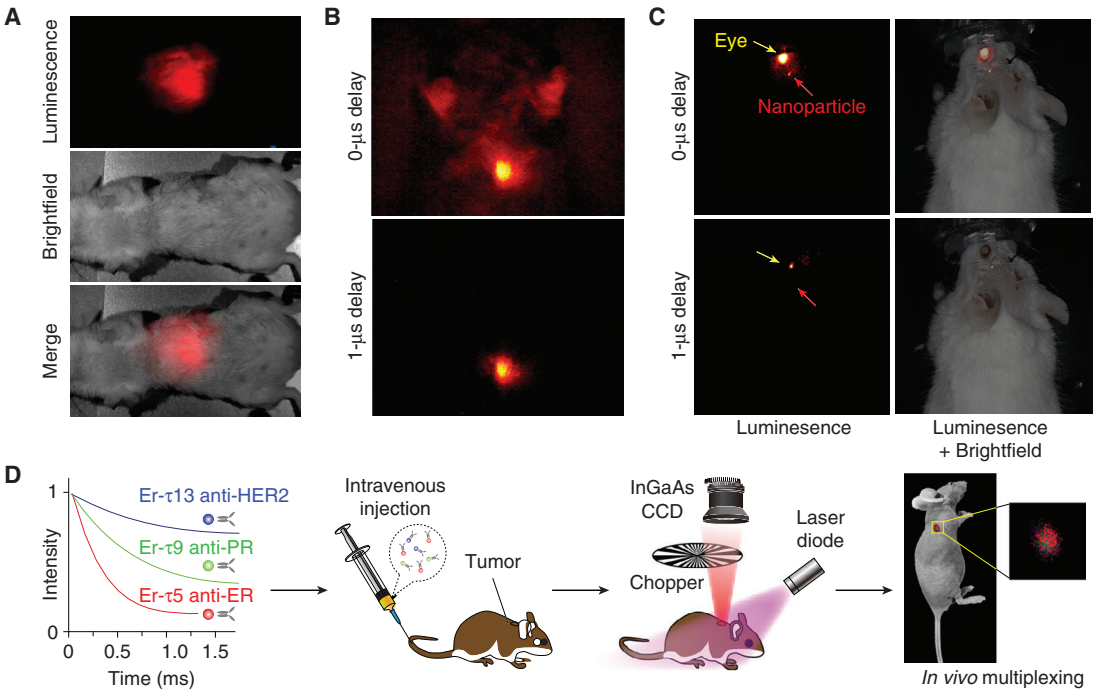


**Figure 7. Photon Upconversion and Deep-Tissue Imaging Using Lanthanide Luminophores**

(A) Whole-animal imaging of a mouse injected via the tail vein with a $Tm^{3+}$-doped photon-upconverting nanoparticle (excitation, 980 nm; emission, 800 nm). Adapted with permission from Chen et al. (2012).

(B) Abdominal imaging of a mouse that has been orally administered $Yb^{3+}$-, $Nd^{3+}$-, and $Tm^{3+}$-containing nanoparticles, which localize initially to the stomach. Micrographs obtained with or without a time delay are shown. Adapted from Tan et al. (2018) under a Creative Commons license.

(C) Imaging of a mouse after intracerebral injection of an $Yb^{3+}$- and $Nd^{3+}$-doped nanoparticle, demonstrating the removal of eye autofluorescence by temporal gating. Adapted from Tan et al. (2018) under a Creative Commons license.

(D) Temporally resolvable τ-dots can be used for multiplexed deep-tissue imaging. Adapted with permission from Fan et al. (2018).

millimeter-sized tumor xenografts in mice (Figure 7D). In principle, this multiplexing technology could be adopted for imaging targets in deeper tissues.

## FUTURE FRONTIERS IN LANTHANIDE LUMINESCENCE

The unique photophysical properties of lanthanide-based probes can be exploited in multiple ways to advance our understanding of biological processes. The application of these metal-based luminophores was once limited to photometric assays, but they are now emerging as versatile tools for biological imaging. We anticipate that the exceptional sensitivity of time-resolved lanthanide luminescence microscopy will be increasingly exploited to visualize low-abundance biomolecules in live cells and animals. Conventional fluorescence microscopy can detect low nanomolar concentrations, which corresponds to a few thousand molecules in a typical mammalian cell. In comparison, the median copy number of mRNAs in mammalian cells is 17 (Schwanhausser et al., 2011). To overcome this limitation, current RNA imaging methods, such as MS2 (Tutucci et al., 2018) or tDeg (Wu et al., 2019) tag recruit several fluorescent proteins to a target; however, this may affect the localization, stability, and function of the transcript. Lanthanide luminophores may afford a general solution for the live imaging of transcripts, as these molecular probes are small in size and their luminescence can be spectrally and temporally resolved from cellular and tissue autofluorescence. We further expect LRET probes will gain popularity as tools for visualizing molecular interactions in living systems. Compared with FRET, LRET enables: (1) longer $R_0$ distances, (2) more accurate distance measurements, and (3) far greater signal-to-noise ratios. For example, LRET could significantly enhance the FRET-based mRNA imaging method developed by the Tyagi group, which utilized short oligonucleotides to juxtapose donor and acceptor molecules upon binding to the targeted transcript (Bratu et al., 2003).

As with any technology, lanthanide-based imaging has room for improvement. On the probe side, the development of less hydrophobic lanthanide chelates is necessary to avoid background from non-specific binding. Appending sulfonic acid groups could render these probes better suited for biological systems as in the case of Alexa Fluor dyes. On the other hand, cell-penetrating probes is also highly desirable. While several lanthanide chelates have been shown to cross the plasma membrane, they are typically sequestered to one or two organelles (Montgomery et al., 2009). A membrane-permeable probe with even distribution throughout the cell is needed. Furthermore, most lanthanide luminophores are excited by UV-A light, and chelates that can be excited by visible light (e.g., 405-nm lasers) could reduce phototoxicity and enable imaging modalities that utilize epi-illumination. While the Yuan group have demonstrated that the BPT antenna (2-(*N*,*N*-diethylanilin-4-yl)-4,6-bis(pyrazol-1-yl)-1,3,5-triazine) can be excited at 420 nm in an aqueous solution,

it requires an auxiliary chelator (Ma et al., 2018; Tian et al., 2014). Combining these moieties into a unimolecular chelate could yield lanthanide probes that are suitable for a wide range of biological applications.

On the instrumentation side, integrating time-gated detection and light-sheet illumination is a logical next step. Light-sheet illumination not only averts long-lived optics background like trans-reflected illumination but also enables optical sectioning of the specimen. Time-resolved light-sheet microscopy would in principle produce images free of biological autofluorescence, optics background, and out-of-plane signals. An imaging platform that can spectrally and temporally unmix lanthanide emissions in real time would also be of great use.

Finally, lanthanide-based optical imaging could be combined with other detection modalities. For example, $Ce^{3+}$ and $Pr^{3+}$ complexes of DTPA-(3,3′-diaminobenzidine)$_2$ have been used for multiplexed electron microscopy (Adams et al., 2016), and analogous probes that utilize brighter trivalent lanthanide ions and 3,3′-diaminobenzidine derivatives with greater molar absorptivity might enable correlative light-electron microscopy. Similarly, lanthanide isotope-labeled antibodies developed for mass spectrometry imaging (Angelo et al., 2014; Giesen et al., 2014) could be modified for optical imaging by adding an antenna group to the DTPA or DOTA chelate. Luminescent lanthanide probes can also double as magnetic resonance imaging contrast agents (Heffern et al., 2014; Song et al., 2019). Multimodal lanthanide imaging will enable us to visualize biological samples at wide-ranging spatial resolutions with the same probe set.

These and other future advances will help establish lanthanide probes as standard components of the biologist's toolbox, enabling new experimental approaches to long-standing problems. Translating lanthanide chemistry into biological discovery will continue to require contributions from multiple fields, including chemical synthesis, photophysics, and microscopy. Chemical biologists will likely be central to these efforts, as they can bridge the development of new lanthanide technologies and their application to cellular and organismal systems.

## SUPPLEMENTAL INFORMATION

Supplemental Information can be found online at https://doi.org/10.1016/j.chembiol.2020.07.009.

## ACKNOWLEDGMENTS

This work was supported by the NIH (R35 GM127030 to J.K.C.) and a Samsung Scholarship (to U.C.).

## SUPPORTING CITATIONS

The following references appear in the Supplemental Information: Mohamadi and Miller, 2016; Moore et al., 2008.

## REFERENCES

Adams, S.R., Mackey, M.R., Ramachandra, R., Lemieux, S.F.P., Steinbach, P., Bushong, E.A., Butko, M.T., Giepmans, B.N.G., Ellisman, M.H., and Tsien, R.Y. (2016). Multicolor electron microscopy for simultaneous visualization of multiple molecular species. Cell Chem Biol. *23*, 1417–1427.

Afsari, H.S., Cardoso Dos Santos, M., Linden, S., Chen, T., Qiu, X., van Bergen En Henegouwen, P.M., Jennings, T.L., Susumu, K., Medintz, I.L., Hildebrandt, N., et al. (2016). Time-gated FRET nanoassemblies for rapid and sensitive intra- and extracellular fluorescence imaging. Sci. Adv. *2*, e1600265.

Algar, W.R., Hildebrandt, N., Vogel, S.S., and Medintz, I.L. (2019). FRET as a biomolecular research tool—understanding its potential while avoiding pitfalls. Nat. Methods *16*, 815–829.

Ali, M.M., Li, F., Zhang, Z., Zhang, K., Kang, D.K., Ankrum, J.A., Le, X.C., and Zhao, W. (2014). Rolling circle amplification: a versatile tool for chemical biology, materials science and medicine. Chem. Soc. Rev. *43*, 3324–3341.

Angelo, M., Bendall, S.C., Finck, R., Hale, M.B., Hitzman, C., Borowsky, A.D., Levenson, R.M., Lowe, J.B., Liu, S.D., Zhao, S., et al. (2014). Multiplexed ion beam imaging of human breast tumors. Nat. Med. *20*, 436–442.

Armelao, L., Quici, S., Barigelletti, F., Accorsi, G., Bottaro, G., Cavazzini, M., and Tondello, E. (2010). Design of luminescent lanthanide complexes: from molecules to highly efficient photo-emitting materials. Coord. Chem. Rev. *254*, 487–505.

Aulsebrook, M.L., Graham, B., Grace, M.R., and Tuck, K.L. (2018). Lanthanide complexes for luminescence-based sensing of low molecular weight analytes. Coord. Chem. Rev. *375*, 191–220.

Baggaley, E., Botchway, S.W., Haycock, J.W., Morris, H., Sazanovich, I.V., Williams, J.A.G., and Weinstein, J.A. (2014). Long-lived metal complexes open up microsecond lifetime imaging microscopy under multiphoton excitation: from FLIM to PLIM and beyond. Chem. Sci. *5*, 879–886.

Bagheri, A., Arandiyan, H., Boyer, C., and Lim, M. (2016). Lanthanide-doped upconversion nanoparticles: emerging intelligent light-activated drug delivery systems. Adv. Sci. (Weinh) *3*, 1500437.

Bajar, B.T., Wang, E.S., Zhang, S., Lin, M.Z., and Chu, J. (2016). A guide to fluorescent protein FRET pairs. Sensors (Basel) *16*, 1488.

Barela, T.D., and Sherry, A.D. (1976). A simple, one-step fluorometric method for determination of nanomolar concentrations of terbium. Anal Biochem. *71*, 351–357.

Barthelmes, D., Barthelmes, K., Schnorr, K., Jonker, H.R.A., Bodmer, B., Allen, K.N., Imperiali, B., and Schwalbe, H. (2017). Conformational dynamics and alignment properties of loop lanthanide-binding-tags (LBTs) studied in interleukin-1β. J. Biomol. NMR *68*, 187–194.

Barthelmes, D., Gränz, M., Barthelmes, K., Allen, K.N., Imperiali, B., Prisner, T., and Schwalbe, H. (2015). Encoded loop-lanthanide-binding tags for long-range distance measurements in proteins by NMR and EPR spectroscopy. J. Biomol. NMR *63*, 275–282.

Beeby, A., Botchway, S.W., Clarkson, I.M., Faulkner, S., Parker, A.W., Parker, D., and Williams, J.A.G. (2000). Luminescence imaging microscopy and lifetime mapping using kinetically stable lanthanide(III) complexes. J. Photochem. Photobiol. B *57*, 83–89.

Beverloo, H.B., van Schadewijk, A., van Gelderen-Boele, S., and Tanke, H.J. (1990). Inorganic phosphors as new luminescent labels for immunocytochemistry and time-resolved microscopy. Cytometry *11*, 784–792.

Bhattacharya, K., Bernasconi, L., and Picard, D. (2018). Luminescence resonance energy transfer between genetically encoded donor and acceptor for protein-protein interaction studies in the molecular chaperone HSP70/HSP90 complexes. Sci. Rep. *8*, 2801.

Bi, S., Yue, S., and Zhang, S. (2017). Hybridization chain reaction: a versatile molecular tool for biosensing, bioimaging, and biomedicine. Chem. Soc. Rev. *46*, 4281–4298.

Bratu, D.P., Cha, B.J., Mhlanga, M.M., Kramer, F.R., and Tyagi, S. (2003). Visualizing the distribution and transport of mRNAs in living cells. Proc. Natl. Acad. Sci. U S A *100*, 13308–13313.

Bünzli, J.-C.G. (2016). Handbook on the Physics and Chemistry of Rare Earths, *vol. 50* (Elsevier).

Cha, A., Snyder, G.E., Selvin, P.R., and Bezanilla, F. (1999). Atomic scale movement of the voltage-sensing region in a potassium channel measured via spectroscopy. Nature *402*, 809–813.

Charbonniere, L.J., Hildebrandt, N., Ziessel, R.F., and Lohmannsroben, H.G. (2006). Lanthanides to quantum dots resonance energy transfer in time-resolved fluoro-immunoassays and luminescence microscopy. J. Am. Chem. Soc. *128*, 12800–12809.

Chen, C., Ao, L., Wu, Y.T., Cifliku, V., Cardoso Dos Santos, M., Bourrier, E., Delbianco, M., Parker, D., Zwier, J.M., Huang, L., et al. (2018). Single-nanoparticle cell barcoding by tunable FRET from lanthanides to quantum dots. Angew. Chem. Int. Ed. *57*, 13686–13690.

Chen, C., Zhang, P., Gao, G., Gao, D., Yang, Y., Liu, H., Wang, Y., Gong, P., and Cai, L. (2014a). Near-infrared-emitting two-dimensional codes based on lattice-strained core/(doped) shell quantum dots with long fluorescence lifetime. Adv. Mater. *26*, 6313–6317.

Chen, C., Zhang, P., Zhang, L., Gao, D., Gao, G., Yang, Y., Li, W., Gong, P., and Cai, L. (2015). Long-decay near-infrared-emitting doped quantum dots for lifetime-based in vivo pH imaging. Chem. Commun. (Camb.) *51*, 11162–11165.

Chen, G., Qiu, H., Prasad, P.N., and Chen, X. (2014b). Upconversion nanoparticles: design, nanochemistry, and applications in theranostics. Chem. Rev. *114*, 5161–5214.

Chen, G., Shen, J., Ohulchanskyy, T.Y., Patel, N.J., Kutikov, A., Li, Z., Song, J., Pandey, R.K., Agren, H., Prasad, P.N., et al. (2012). (α-NaYbF4:Tm(3+))/CaF2 core/shell nanoparticles with efficient near-infrared to near-infrared upconversion for high-contrast deep tissue bioimaging. ACS Nano *6*, 8280–8287.

Chen, J., and Selvin, P.R. (2000a). Lifetime- and color-tailored fluorophores in the micro- to millisecond time regime. J. Am. Chem. Soc. *122*, 657–660.

Chen, J., and Selvin, P.R. (2000b). Synthesis of 7-amino-4-trifluoromethyl-2-(1H)-quinolinone and its use as an antenna molecule for luminescent europium polyaminocarboxylates chelates. J. Photochem. Photobiol. A *135*, 27–32.

Cho, U., Riordan, D.P., Ciepla, P., Kocherlakota, K.S., Chen, J.K., and Harbury, P.B. (2018). Ultrasensitive optical imaging with lanthanide lumiphores. Nat. Chem. Biol. *14*, 15–21.

Cotruvo, J.A., Featherston, E.R., Mattocks, J.A., Ho, J.V., and Laremore, T.N. (2018). Lanmodulin: a highly selective lanthanide-binding protein from a lanthanide-utilizing bacterium. J. Am. Chem. Soc. *140*, 15056–15061.

Cui, W., and Parker, L.L. (2016). Modular, antibody-free time-resolved LRET kinase assay enabled by quantum dots and Tb(3+)-sensitizing peptides. Sci. Rep. *6*, 28971.

Dai, Z., Tian, L., Song, B., Liu, X., and Yuan, J. (2017). Development of a novel lysosome-targetable time-gated luminescence probe for ratiometric and luminescence lifetime detection of nitric oxide in vivo. Chem. Sci. *8*, 1969–1976.

Day, R.N., and Davidson, M.W. (2009). The fluorescent protein palette: tools for cellular imaging. Chem. Soc. Rev. *38*, 2887–2921.

Diao, S., Blackburn, J.L., Hong, G., Antaris, A.L., Chang, J., Wu, J.Z., Zhang, B., Cheng, K., Kuo, C.J., and Dai, H. (2015). Fluorescence imaging *in vivo* at wavelengths beyond 1500 nm. Angew. Chem. Int. Ed. *54*, 14758–14762.

Dickson, E.F., Pollak, A., and Diamandis, E.P. (1995). Time-resolved detection of lanthanide luminescence for ultrasensitive bioanalytical assays. J. Photochem. Photobiol. B *27*, 3–19.

Ding, F., Zhan, Y., Lu, X., and Sun, Y. (2018). Recent advances in near-infrared II fluorophores for multifunctional biomedical imaging. Chem. Sci. *9*, 4370–4380.

Dong, H., Du, S.R., Zheng, X.Y., Lyu, G.M., Sun, L.D., Li, L.D., Zhang, P.Z., Zhang, C., and Yan, C.H. (2015). Lanthanide nanoparticles: from design toward bioimaging and therapy. Chem. Rev. *115*, 10725–10815.

Emami-Nemini, A., Roux, T., Leblay, M., Bourrier, E., Lamarque, L., Trinquet, E., and Lohse, M.J. (2013). Time-resolved fluorescence ligand binding for G protein-coupled receptors. Nat. Protoc. *8*, 1307–1320.

Faklaris, O., Cottet, M., Falco, A., Villier, B., Laget, M., Zwier, J.M., Trinquet, E., Mouillac, B., Pin, J.P., and Durroux, T. (2015). Multicolor time-resolved Förster resonance energy transfer microscopy reveals the impact of GPCR oligomerization on internalization processes. FASEB J. *29*, 2235–2246.

Fan, Y., Wang, P., Lu, Y., Wang, R., Zhou, L., Zheng, X., Li, X., Piper, J.A., and Zhang, F. (2018). Lifetime-engineered NIR-II nanoparticles unlock multiplexed in vivo imaging. Nat. Nanotechnol. *13*, 941–946.

Feuchtinger, A., Walch, A., and Dobosz, M. (2016). Deep tissue imaging: a review from a preclinical cancer research perspective. Histochem. Cell Biol. *146*, 781–806.

Firsching, F.H., and Brune, S.N. (1991). Solubility products of the trivalent rare-earth phosphates. J. Chem. Eng. Data *36*, 93–95.

Franz, K.J., Nitz, M., and Imperiali, B. (2003). Lanthanide-binding tags as versatile protein coexpression probes. Chembiochem *4*, 265–271.

Furukawa, K., Takahashi, Y., and Sata, H. (2007). Effect of the formation of EDTA complexes on the diffusion of metal ions in water. Geochim Cosmochim Acta *71*, 4416–4424.

Gahlaut, N., and Miller, L.W. (2010). Time-resolved microscopy for imaging lanthanide luminescence in living cells. Cytometry A *77*, 1113–1125.

Gáspári, Z., and Perczel, A. (2010). Protein dynamics as reported by NMR. In Annual Reports on NMR Spectroscopy, G.A. Webb, ed. (Elsevier), pp. 35–75.

Ge, P., and Selvin, P.R. (2004). Carbostyril derivatives as antenna molecules for luminescent lanthanide chelates. Bioconjug. Chem. *15*, 1088–1094.

Ge, P., and Selvin, P.R. (2008). New 9- or 10-dentate luminescent lanthanide chelates. Bioconjug. Chem. *19*, 1105–1111.

Gee, A., and Xu, X. (2018). Surface functionalisation of upconversion nanoparticles with different moieties for biomedical applications. Surfaces *1*, 96–121.

Geissler, D., Charbonniere, L.J., Ziessel, R.F., Butlin, N.G., Lohmannsroben, H.G., and Hildebrandt, N. (2010). Quantum dot biosensors for ultrasensitive multiplexed diagnostics. Angew. Chem. Int. Ed. *49*, 1396–1401.

Geissler, D., Stufler, S., Lohmannsroben, H.G., and Hildebrandt, N. (2013). Six-color time-resolved Forster resonance energy transfer for ultrasensitive multiplexed biosensing. J. Am. Chem. Soc. *135*, 1102–1109.

George Abraham, B., Sarkisyan, K.S., Mishin, A.S., Santala, V., Tkachenko, N.V., and Karp, M. (2015). Fluorescent protein based FRET pairs with improved dynamic range for fluorescence lifetime measurements. PLoS One *10*, e0134436.

Gerver, R.E., Gomez-Sjoberg, R., Baxter, B.C., Thorn, K.S., Fordyce, P.M., Diaz-Botia, C.A., Helms, B.A., and DeRisi, J.L. (2012). Programmable microfluidic synthesis of spectrally encoded microspheres. Lab A Chip *12*, 4716–4723.

Giesen, C., Wang, H.A., Schapiro, D., Zivanovic, N., Jacobs, A., Hattendorf, B., Schuffler, P.J., Grolimund, D., Buhmann, J.M., Brandt, S., et al. (2014). Highly multiplexed imaging of tumor tissues with subcellular resolution by mass cytometry. Nat. Methods *11*, 417–422.

Gonzalez, J., Rambhadran, A., Du, M., and Jayaraman, V. (2008). LRET investigations of conformational changes in the ligand binding domain of a functional AMPA receptor. Biochemistry *47*, 10027–10032.

Gueimonde, M., Tolkko, S., Korpimaki, T., and Salminen, S. (2004). New real-time quantitative PCR procedure for quantification of bifidobacteria in human fecal samples. Appl. Environ. Microbiol. *70*, 4165–4169.

Güzel, Y., Rainer, M., Mirza, M.R., and Bonn, G.K. (2012). Highly efficient precipitation of phosphoproteins using trivalent europium, terbium, and erbium ions. Anal Bioanal. Chem. *403*, 1323–1331.

Hanaoka, K., Kikuchi, K., Kobayashi, S., and Nagano, T. (2007). Time-resolved long-lived luminescence imaging method employing luminescent lanthanide probes with a new microscopy system. J. Am. Chem. Soc. *129*, 13502–13509.

Heffern, M.C., Matosziuk, L.M., and Meade, T.J. (2014). Lanthanide probes for bioresponsive imaging. Chem. Rev. *114*, 4496–4539.

Hemmilä, I. (1985). Fluoroimmunoassays and immunofluorometric assays. Clin. Chem. *31*, 359–370.

Hemmilä, I. (1988). Lanthanides as probes for time-resolved fluorometric immunoassays. Scand. J. Clin. Lab. Invest. *48*, 389–399.

Hemmilä, I., Dakubu, S., Mukkala, V.M., Siitari, H., and Lövgren, T. (1984). Europium as a label in time-resolved immunofluorometric assays. Anal Biochem. *137*, 335–343.

Hewitt, S.H., Parris, J., Mailhot, R., and Butler, S.J. (2017). A continuous luminescence assay for monitoring kinase activity: signalling the ADP/ATP ratio using a discrete europium complex. Chem. Commun. (Camb.) *53*, 12626–12629.

Hildebrandt, N., Charbonniere, L.J., Beck, M., Ziessel, R.F., and Lohmannsroben, H.G. (2005). Quantum dots as efficient energy acceptors in a time-resolved fluoroimmunoassay. Angew. Chem. Int. Ed. *44*, 7612–7615.

Hochreiter, B., Garcia, A.P., and Schmid, J.A. (2015). Fluorescent proteins as genetically encoded FRET biosensors in life sciences. Sensors (Basel) *15*, 26281–26314.

Hogue, C.W., MacManus, J.P., Banville, D., and Szabo, A.G. (1992). Comparison of terbium (III) luminescence enhancement in mutants of EF hand calcium binding proteins. J. Biol. Chem. *267*, 13340–13347.

Horrocks, W.D., Jr., Schmidt, G.F., Sudnick, D.R., Kittrell, C., and Bernheim, R.A. (1977). Laser-induced lanthanide ion luminescence lifetime measurements by direct excitation of metal ion levels. A new class of structural probe for calcium-binding proteins and nucleic acids. J. Am. Chem. Soc. *99*, 2378–2380.

Jin, D., Connally, R., and Piper, J. (2007a). Practical time-gated luminescence flow cytometry. I: concepts. Cytometry A *71*, 783–796.

Jin, D., Connally, R., and Piper, J. (2007b). Practical time-gated luminescence flow cytometry. II: experimental evaluation using UV LED excitation. Cytometry A *71*, 797–808.

Jin, D., and Piper, J.A. (2011). Time-gated luminescence microscopy allowing direct visual inspection of lanthanide-stained microorganisms in background-free condition. Anal Chem. *83*, 2294–2300.

Kamimura, M., Matsumoto, T., Suyari, S., Umezawa, M., and Soga, K. (2017). Ratiometric near-infrared fluorescence nanothermometry in the OTN-NIR (NIR II/III) biological window based on rare-earth doped β-NaYF 4 nanoparticles. J. Mater. Chem. B *5*, 1917–1925.

Kubota, T., Durek, T., Dang, B., Finol-Urdaneta, R.K., Craik, D.J., Kent, S.B., French, R.J., Bezanilla, F., and Correa, A.M. (2017). Mapping of voltage sensor positions in resting and inactivated mammalian sodium channels by LRET. Proc. Natl. Acad. Sci. U S A. *114*, E1857–E1865.

Kubota, T., Lacroix, J.J., Bezanilla, F., and Correa, A.M. (2014). Probing α-3(10) transitions in a voltage-sensing S4 helix. Biophys. J. *107*, 1117–1128.

Lan, T.-H., Wu, G., and Lambert, N.A. (2015). Lateral diffusion contributes to FRET from lanthanide-tagged membrane proteins. Biochem. Biophys. Res. Commun. *464*, 244–248.

Leder, R.O., Helgerson, S.L., and Thomas, D.D. (1989). The transverse location of the retinal chromophore in the purple membrane by diffusion-enhanced energy transfer. J. Mol. Biol. *209*, 683–701.

Levoye, A., Zwier, J.M., Jaracz-Ros, A., Klipfel, L., Cottet, M., Maurel, D., Bdioui, S., Balabanian, K., Prézeau, L., Trinquet, E., et al. (2015). A broad G protein-coupled receptor internalization assay that combines SNAP-tag labeling, diffusion-enhanced resonance energy transfer, and a highly emissive terbium cryptate. Front Endocrinol. (Lausanne) *6*, 167.

Li, M., and Selvin, P.R. (1995). Luminescent polyaminocarboxylate chelates of terbium and europium: the effect of chelate structure. J. Am. Chem. Soc. *117*, 8132–8138.

Li, M., and Selvin, P.R. (1997). Amine-reactive forms of a luminescent diethylenetriaminepentaacetic acid chelate of terbium and europium: attachment to DNA and energy transfer measurements. Bioconjug. Chem. *8*, 127–132.

Liu, Q., Sun, Y., Yang, T., Feng, W., Li, C., and Li, F. (2011). Sub-10 nm hexagonal lanthanide-doped NaLuF4 upconversion nanocrystals for sensitive bioimaging in vivo. J. Am. Chem. Soc. *133*, 17122–17125.

Liu, X., Guo, L., Song, B., Tang, Z., and Yuan, J. (2017). Development of a novel europium complex-based luminescent probe for time-gated luminescence imaging of hypochlorous acid in living samples. Methods Appl. Fluoresc. *5*, 014009.

Lo, K.K., Choi, A.W., and Law, W.H. (2012). Applications of luminescent inorganic and organometallic transition metal complexes as biomolecular and cellular probes. Dalton Trans. *41*, 6021–6047.

Lu, Y., Lu, J., Zhao, J., Cusido, J., Raymo, F.M., Yuan, J., Yang, S., Leif, R.C., Huo, Y., Piper, J.A., et al. (2014a). On-the-fly decoding luminescence lifetimes in the microsecond region for lanthanide-encoded suspension arrays. Nat. Commun. *5*, 3741.

Lu, Y., Zhao, J., Zhang, R., Liu, Y., Liu, D., Goldys, E.M., Yang, X., Xi, P., Sunna, A., Lu, J., et al. (2014b). Tunable lifetime multiplexing using luminescent nanocrystals. Nat. Photon. *8*, 32–36.

Ma, H., Song, B., Wang, Y., Cong, D., Jiang, Y., and Yuan, J. (2017). Dual-emissive nanoarchitecture of lanthanide-complex-modified silica particles for in vivo ratiometric time-gated luminescence imaging of hypochlorous acid. Chem. Sci. *8*, 150–159.

Ma, H., Wang, X., Song, B., Wang, L., Tang, Z., Luo, T., and Yuan, J. (2018). Extending the excitation wavelength from UV to visible light for a europium complex-based mitochondria targetable luminescent probe for singlet oxygen. Dalton Trans. *47*, 12852–12857.

Maltman, B.A., Dunsmore, C.J., Couturier, S.C., Tirnaveanu, A.E., Delbederi, Z., McMordie, R.A., Naredo, G., Ramage, R., and Cotton, G. (2010). 9-Aminoacridine peptide derivatives as versatile reporter systems for use in fluorescence lifetime assays. Chem. Commun. (Camb.) *46*, 6929–6931.

Marriott, G., Heidecker, M., Diamandis, E.P., and Yan-Marriott, Y. (1994). Time-resolved delayed luminescence image microscopy using an europium ion chelate complex. Biophys. J. *67*, 957–965.

Martin, L.J., Hähnke, M.J., Nitz, M., Wöhnert, J., Silvaggi, N.R., Allen, K.N., Schwalbe, H., and Imperiali, B. (2007). Double-lanthanide-binding tags: design, photophysical properties, and NMR applications. J. Am. Chem. Soc. *129*, 7106–7113.

Martin, L.J., Sculimbrene, B.R., Nitz, M., and Imperiali, B. (2005). Rapid combinatorial screening of peptide libraries for the selection of lanthanide-binding tags (LBTs). QSAR Comb. Sci. *24*, 1149–1157.

Mathis, G. (1993). Rare earth cryptates and homogeneous fluoroimmunoassays with human sera. Clin. Chem. *39*, 1953–1959.

Mathis, G. (1995). Probing molecular interactions with homogeneous techniques based on rare earth cryptates and fluorescence energy transfer. Clin. Chem. *41*, 1391–1397.

Mathis, G., and Bazin, H. (2010). Stable luminescent chelates and macrocyclic compounds. In Lanthanide Luminescence, P. Hänninen and H. Härmä, eds. (Springer), pp. 47–88.

Mohamadi, A., and Miller, L.W. (2016). Brightly luminescent and kinetically inert lanthanide bioprobes based on linear and preorganized chelators. Bioconjug. Chem. *27*, 2540–2548.

Montgomery, C.P., Murray, B.S., New, E.J., Pal, R., and Parker, D. (2009). Cell-penetrating metal complex optical probes: targeted and responsive systems based on lanthanide luminescence. Acc. Chem. Res. *42*, 925–937.

Moore, E.G., Samuel, A.P., and Raymond, K.N. (2009). From antenna to assay: lessons learned in lanthanide luminescence. Acc. Chem. Res. *42*, 542–552.

Moore, E.G., Xu, J., Jocher, C.J., Castro-Rodriguez, I., and Raymond, K.N. (2008). Highly luminescent lanthanide complexes of 1-hydroxy-2-pyridinones. Inorg. Chem. *47*, 3105–3118.

Morrison, J.F., and Cleland, W. (1983). Lanthanide-adenosine 5'-triphosphate complexes: determination of their dissociation constants and mechanism of action as inhibitors of yeast hexokinase. Biochemistry *22*, 5507–5513.

Mukkala, V.M., Helenius, M., Hemmilä, I., Kankare, J., and Takalo, H. (1993). Development of luminescent europium (III) and terbium (III) chelates of 2,2′:6′,2″-terpyridine derivatives for protein labelling. Helvetica Chim. Acta *76*, 1361–1378.

Mukkala, V.M., Liitti, P., Hemmilä, I., Takalo, H., Matachescu, C., and Kankare, J. (1996). Novel thiazole-containing complexing agents and luminescence of their europum (III) and terbium (III) chelates. Helvetica Chim. Acta *79*, 295–306.

Müller, S.M., Galliardt, H., Schneider, J., Barisas, B.G., and Seidel, T. (2013). Quantification of Förster resonance energy transfer by monitoring sensitized emission in living plant cells. Front Plant Sci. *4*, 413.

Nau, W.M., and Zhang, X.Y. (1999). An exceedingly long-lived fluorescent state as a distinct structural and dynamic probe for supramolecular association: an exploratory study of host-guest complexation by cyclodextrins. J. Am. Chem. Soc. *121*, 8022–8032.

Nguyen, H.Q., Baxter, B.C., Brower, K., Diaz-Botia, C.A., DeRisi, J.L., Fordyce, P.M., and Thorn, K.S. (2017). Programmable microfluidic synthesis of over one thousand uniquely identifiable spectral codes. Adv. Opt. Mater. *5*, 1600548.

Nguyen, H.Q., Roy, J., Harink, B., Damle, N.P., Latorraca, N.R., Baxter, B.C., Brower, K., Longwell, S.A., Kortemme, T., Thorn, K.S., et al. (2019). Quantitative mapping of protein-peptide affinity landscapes using spectrally encoded beads. Elife *8*, e40499.

Nieboer, E. (1975). The lanthanide ions as structural probes in biological and model systems. In Rare Earths (Springer), pp. 1–47.

Nishioka, T., Yuan, J., Yamamoto, Y., Sumitomo, K., Wang, Z., Hashino, K., Hosoya, C., Ikawa, K., Wang, G., and Matsumoto, K. (2006). New luminescent europium(III) chelates for DNA labeling. Inorg. Chem. *45*, 4088–4096.

Nitsche, J.M., Chang, H.C., Weber, P.A., and Nicholson, B.J. (2004). A transient diffusion model yields unitary gap junctional permeabilities from images of cell-to-cell fluorescent dye transfer between *Xenopus* oocytes. Biophys. J. *86*, 2058–2077.

Nurmi, J., Wikman, T., Karp, M., and Lovgren, T. (2002). High-performance real-time quantitative RT-PCR using lanthanide probes and a dual-temperature hybridization assay. Anal Chem. *74*, 3525–3532.

Nurmi, J., Ylikoski, A., Soukka, T., Karp, M., and Lovgren, T. (2000). A new label technology for the detection of specific polymerase chain reaction products in a closed tube. Nucleic Acids Res. *28*, E28.

Ogata, A., Tagoh, H., Lee, T., Kuritani, T., Takahara, Y., Shimamura, T., Ikegami, H., Kurimoto, M., Yoshizaki, K., and Kishimoto, T. (1992). A new highly sensitive immunoassay for cytokines by dissociation-enhanced lanthanide fluoroimmunoassay (DELFIA). J. Immunol. Methods *148*, 15–22.

Ortega, G., Pons, M., and Millet, O. (2013). Protein functional dynamics in multiple timescales as studied by NMR spectroscopy. In Advances in Protein Chemistry and Structural Biology, T. Karabencheva-Christova, ed. (Elsevier), pp. 219–251.

Parker, D., and Williams, J.A.G. (1996). Getting excited about lanthanide complexation chemistry. J. Chem. Soc. Dalton Trans. 3613–3628.

Patsenker, L.D., Tatarets, A.L., Povrozin, Y.A., and Terpetschnig, E.A. (2011). Long-wavelength fluorescence lifetime labels. Bioanal. Rev. *3*, 115–137.

Piatkevich, K.D., and Verkhusha, V.V. (2011). Guide to red fluorescent proteins and biosensors for flow cytometry. Methods Cell Biol. *102*, 431–461.

Pichon, X., Lagha, M., Mueller, F., and Bertrand, E. (2018). A growing toolbox to image gene expression in single cells: sensitive approaches for demanding challenges. Mol. Cell *71*, 468–480.

Pillai, S., Kozlov, M., Marras, S.A., Krasnoperov, L.N., and Mustaev, A. (2012). New cross-linking quinoline and quinolone derivatives for sensitive fluorescent labeling. J. Fluoresc *22*, 1021–1032.

Pou, C., la Cour, C.M., Stoddart, L.A., Millan, M.J., and Milligan, G. (2012). Functional homomers and heteromers of dopamine D2L and D3 receptors co-exist at the cell surface. J. Biol. Chem. *287*, 8864–8878.

Power, R.M., and Huisken, J. (2017). A guide to light-sheet fluorescence microscopy for multiscale imaging. Nat. Methods *14*, 360–373.

Rajapakse, H.E., Gahlaut, N., Mohandessi, S., Yu, D., Turner, J.R., and Miller, L.W. (2010). Time-resolved luminescence resonance energy transfer imaging of protein-protein interactions in living cells. Proc. Natl. Acad. Sci. U S A. *107*, 13582–13587.

Rajendran, M., and Miller, L.W. (2015). Evaluating the performance of time-gated live-cell microscopy with lanthanide probes. Biophys. J. *109*, 240–248.

Rajendran, M., Yapici, E., and Miller, L.W. (2014). Lanthanide-based imaging of protein-protein interactions in live cells. Inorg. Chem. *53*, 1839–1853.

Reynolds, A.M., Sculimbrene, B.R., and Imperiali, B. (2008). Lanthanide-binding tags with unnatural amino acids: sensitizing $Tb^{3+}$ and $Eu^{3+}$ luminescence at longer wavelengths. Bioconjug. Chem. *19*, 588–591.

Rich, R.M., Stankowska, D.L., Maliwal, B.P., Sorensen, T.J., Laursen, B.W., Krishnamoorthy, R.R., Gryczynski, Z., Borejdo, J., Gryczynski, I., and Fudala, R. (2013). Elimination of autofluorescence background from fluorescence tissue images by use of time-gated detection and the AzaDiOxaTriAngulenium (ADOTA) fluorophore. Anal Bioanal. Chem. *405*, 2065–2075.

Rocha, J., Carlos, L.D., Paz, F.A., and Ananias, D. (2011). Luminescent multifunctional lanthanides-based metal-organic frameworks. Chem. Soc. Rev. *40*, 926–940.

Rodriguez, E.A., Campbell, R.E., Lin, J.Y., Lin, M.Z., Miyawaki, A., Palmer, A.E., Shu, X., Zhang, J., and Tsien, R.Y. (2017). The growing and glowing toolbox of fluorescent and photoactive proteins. Trends Biochem. Sci. *42*, 111–129.

Schwanhausser, B., Busse, D., Li, N., Dittmar, G., Schuchhardt, J., Wolf, J., Chen, W., and Selbach, M. (2011). Global quantification of mammalian gene expression control. Nature *473*, 337–342.

Selvin, P.R. (1996). Lanthanide-based resonance energy transfer. IEEE J. Sel. Top. Quantum Electron. *2*, 1077–1087.

Selvin, P.R., and Hearst, J.E. (1994). Luminescence energy transfer using a terbium chelate: improvements on fluorescence energy transfer. Proc. Natl. Acad. Sci. U S A. *91*, 10024–10028.

Selvin, P.R., Rana, T.M., and Hearst, J.E. (1994). Luminescence resonance energy transfer. J. Am. Chem. Soc. *116*, 6029–6030.

Seveus, L., Väisälä, M., Syrjänen, S., Sandberg, M., Kuusisto, A., Harju, R., Salo, J., Hemmilä, I., Kojola, H., and Soini, E. (1992). Time-resolved fluorescence imaging of europium chelate label in immunohistochemistry and in situ hybridization. Cytometry *13*, 329–338.

Shuvaev, S., Starck, M., and Parker, D. (2017). Responsive, water-soluble europium(III) luminescent probes. Chem. Eur. J. *23*, 9974–9989.

Sigal, Y.M., Zhou, R., and Zhuang, X. (2018). Visualizing and discovering cellular structures with super-resolution microscopy. Science *361*, 880–887.

Silvaggi, N.R., Martin, L.J., Schwalbe, H., Imperiali, B., and Allen, K.N. (2007). Double-lanthanide-binding tags for macromolecular crystallographic structure determination. J. Am. Chem. Soc. *129*, 7114–7120.

Smith, J.A., West, R.M., and Allen, M. (2004). Acridones and quinacridones: novel fluorophores for fluorescence lifetime studies. J. Fluoresc *14*, 151–171.

Soini, A.E., Kuusisto, A., Meltola, N.J., Soini, E., and Seveus, L. (2003). A new technique for multiparameter imaging microscopy: use of long decay time photoluminescent labels enables multiple color immunocytochemistry with low channel-to-channel crosstalk. Microsc. Res. Tech. *62*, 396–407.

Soini, E., and Kojola, H. (1983). Time-resolved fluorometer for lanthanide chelates—a new generation of nonisotopic immunoassays. Clin. Chem. *29*, 65–68.

Song, B., Shi, W., Shi, W., Qin, X., Ma, H., Tan, M., Zhang, W., Guo, L., and Yuan, J. (2019). A dual-modal nanoprobe based on Eu(III) complex-$MnO_2$ nanosheet nanocomposites for time-gated luminescence-magnetic resonance imaging of glutathione in vitro and in vivo. Nanoscale *11*, 6784–6793.

Song, B., Ye, Z., Yang, Y., Ma, H., Zheng, X., Jin, D., and Yuan, J. (2015). Background-free in-vivo imaging of vitamin C using time-gateable responsive probe. Sci. Rep. *5*, 14194.

Spitzer, M.H., and Nolan, G.P. (2016). Mass cytometry: single cells, many features. Cell *165*, 780–791.

Sun, J., Song, B., Ye, Z., and Yuan, J. (2015). Mitochondria targetable time-gated luminescence probe for singlet oxygen based on a β-diketonate-europium complex. Inorg. Chem. *54*, 11660–11668.

Takalo, H., Mukkala, V.M., Meriö, L., Rodríguez-Ubis, J.C., Sedano, R., Juanes, O., and Brunet, E. (1997). Development of luminescent terbium (III) chelates for protein labelling: effect of triplet-state energy level. Helvetica Chim. Acta *80*, 372–387.

Tan, M., Del Rosal, B., Zhang, Y., Martín Rodríguez, E., Hu, J., Zhou, Z., Fan, R., Ortgies, D.H., Fernández, N., Chaves-Coira, I., et al. (2018). Rare-earth-doped fluoride nanoparticles with engineered long luminescence lifetime for time-gated in vivo optical imaging in the second biological window. Nanoscale *10*, 17771–17780.

Tang, Z., Song, B., Ma, H., Luo, T., Guo, L., and Yuan, J. (2019a). Mitochondria-targetable ratiometric time-gated luminescence probe for carbon monoxide based on lanthanide complexes. Anal Chem. *91*, 2939–2946.

Tang, Z., Song, B., Zhang, W., Guo, L., and Yuan, J. (2019b). Precise monitoring of drug-induced kidney injury using an endoplasmic reticulum-targetable ratiometric time-gated luminescence probe for superoxide anions. Anal Chem. *91*, 14019–14028.

Thomas, D.D., Carlsen, W.F., and Stryer, L. (1978). Fluorescence energy transfer in the rapid-diffusion limit. Proc. Natl. Acad. Sci. U S A. *75*, 5746–5750.

Tian, L., Dai, Z., Liu, X., Song, B., Ye, Z., and Yuan, J. (2015). Ratiometric time-gated luminescence probe for nitric oxide based on an apoferritin-assembled lanthanide complex-rhodamine luminescence resonance energy transfer system. Anal Chem. *87*, 10878–10885.

Tian, L., Dai, Z., Ye, Z., Song, B., and Yuan, J. (2014). Preparation and functionalization of a visible-light-excited europium complex-modified luminescent protein for cell imaging applications. Analyst *139*, 1162–1167.

Tu, C.C., Chen, K.P., Yang, T.A., Chou, M.Y., Lin, L.Y., and Li, Y.K. (2016). Silicon quantum dot nanoparticles with antifouling coatings for immunostaining on live cancer cells. ACS Appl. Mater. Interfaces *8*, 13714–13723.

Tutucci, E., Vera, M., Biswas, J., Garcia, J., Parker, R., and Singer, R.H. (2018). An improved MS2 system for accurate reporting of the mRNA life cycle. Nat. Methods *15*, 81–89.

Vereb, G., Jares-Erijman, E., Selvin, P.R., and Jovin, T.M. (1998). Temporally and spectrally resolved imaging microscopy of lanthanide chelates. Biophys. J. *74*, 2210–2222.

Wang, F., and Liu, X. (2009). Recent advances in the chemistry of lanthanide-doped upconversion nanocrystals. Chem. Soc. Rev. *38*, 976–989.

Wang, L., Frei, M.S., Salim, A., and Johnsson, K. (2019). Small-molecule fluorescent probes for live-cell super-resolution microscopy. J. Am. Chem. Soc. *141*, 2770–2781.

Wang, L.V., and Yao, J. (2016). A practical guide to photoacoustic tomography in the life sciences. Nat. Methods *13*, 627–638.

Wawrzinek, R., Ziomkowska, J., Heuveling, J., Mertens, M., Herrmann, A., Schneider, E., and Wessig, P. (2013). DBD dyes as fluorescence lifetime probes to study conformational changes in proteins. Chemistry *19*, 17349–17357.

Weissman, S. (1942). Intramolecular energy transfer the fluorescence of complexes of europium. J. Chem. Phys. *10*, 214–217.

Welch, J.T., Kearney, W.R., and Franklin, S.J. (2003). Lanthanide-binding helix-turn-helix peptides: solution structure of a designed metallonuclease. Proc. Natl. Acad. Sci. U S A. *100*, 3725–3730.

Wen, S., Zhou, J., Zheng, K., Bednarkiewicz, A., Liu, X., and Jin, D. (2018). Advances in highly doped upconversion nanoparticles. Nat. Commun. *9*, 2415.

Whittaker, M., Wilson-Kubalek, E.M., Smith, J.E., Faust, L., Milligan, R.A., and Sweeney, H.L. (1995). A 35-Å movement of smooth muscle myosin on ADP release. Nature *378*, 748–751.

Wigington, C.P., Roy, J., Damle, N.P., Yadav, V.K., Blikstad, C., Resch, E., Wong, C.J., Mackay, D.R., Wang, J.T., Krystkowiak, I., et al. (2019). Systematic discovery of short linear motifs decodes calcineurin phosphatase signaling. bioRxiv, 632547, https://doi.org/10.1016/j.molcel.2020.06.029.

Wöhnert, J., Franz, K.J., Nitz, M., Imperiali, B., and Schwalbe, H. (2003). Protein alignment by a coexpressed lanthanide-binding tag for the measurement of residual dipolar couplings. J. Am. Chem. Soc. *125*, 13338–13339.

Wu, J., Zaccara, S., Khuperkar, D., Kim, H., Tanenbaum, M.E., and Jaffrey, S.R. (2019). Live imaging of mRNA using RNA-stabilized fluorogenic proteins. Nat. Methods *16*, 862–865.

Wu, P., and Yan, X.P. (2013). Doped quantum dots for chemo/biosensing and bioimaging. Chem. Soc. Rev. *42*, 5489–5521.

Wu, X., Chen, G., Shen, J., Li, Z., Zhang, Y., and Han, G. (2015). Upconversion nanoparticles: a versatile solution to multiscale biological imaging. Bioconjug. Chem. *26*, 166–175.

Xiao, M., Reifenberger, J.G., Wells, A.L., Baldacchino, C., Chen, L.Q., Ge, P., Sweeney, H.L., and Selvin, P.R. (2003). An actin-dependent conformational change in myosin. Nat. Struct. Biol. *10*, 402–408.

Xiao, M., and Selvin, P.R. (2001). Quantum yields of luminescent lanthanide chelates and far-red dyes measured by resonance energy transfer. J. Am. Chem. Soc. *123*, 7067–7073.

Xiao, X., Haushalter, J.P., Kotz, K.T., and Faris, G.W. (2011). Cell assay using a two-photon-excited europium chelate. Biomed. Opt. Express *2*, 2255–2264.

Xu, H., Cao, C.S., Kang, X.M., and Zhao, B. (2016). Lanthanide-based metal-organic frameworks as luminescent probes. Dalton Trans. *45*, 18003–18017.

Xu, J., Corneillie, T.M., Moore, E.G., Law, G.L., Butlin, N.G., and Raymond, K.N. (2011). Octadentate cages of Tb(III) 2-hydroxyisophthalamides: a new standard for luminescent lanthanide labels. J. Am. Chem. Soc. *133*, 19900–19910.

Xue, Z., Zeng, S., and Hao, J. (2018). Non-invasive through-skull brain vascular imaging and small tumor diagnosis based on NIR-II emissive lanthanide nanoprobes beyond 1500nm. Biomaterials *171*, 153–163.

Yam, V.W., and Wong, K.M. (2011). Luminescent metal complexes of d6, d8 and d10 transition metal centres. Chem. Commun. (Camb.) *47*, 11579–11592.

Yang, W., Srivastava, P.K., Han, S., Jing, L., Tu, C.C., and Chen, S.L. (2019). Optomechanical time-gated fluorescence imaging using long-lived silicon quantum dot nanoparticles. Anal Chem. *91*, 5499–5503.

Ye, Z., Xiao, Y., Song, B., and Yuan, J. (2014). Design and synthesis of a new terbium complex-based luminescent probe for time-resolved luminescence sensing of zinc ions. J. Fluoresc *24*, 1537–1544.

Zhang, B., Yang, C., Gao, Y., Wang, Y., Bu, C., Hu, S., Liu, L., Demir, H.V., Qu, J., and Yong, K.T. (2017). Engineering quantum dots with different emission wavelengths and specific fluorescence lifetimes for spectrally and temporally multiplexed imaging of cells. Nanotheranostics *1*, 131–140.

Zhang, L., Chen, C., Li, W., Gao, G., Gong, P., and Cai, L. (2016). Living cell multilifetime encoding based on lifetime-tunable lattice-strained quantum dots. ACS Appl. Mater. Interfaces *8*, 13187–13191.

Zhang, L., Zheng, X., Deng, W., Lu, Y., Lechevallier, S., Ye, Z., Goldys, E.M., Dawes, J.M., Piper, J.A., Yuan, J., et al. (2014a). Practical implementation, characterization and applications of a multi-colour time-gated luminescence microscope. Sci. Rep. *4*, 6597.

Zhang, M., Yue, J., Cui, R., Ma, Z., Wan, H., Wang, F., Zhu, S., Zhou, Y., Kuang, Y., Zhong, Y., et al. (2018). Bright quantum dots emitting at ~1,600 nm in the NIR-IIb window for deep tissue fluorescence imaging. Proc. Natl. Acad. Sci. U S A. *115*, 6590–6595.

Zhang, S., Garcia-D'Angeli, A., Brennan, J.P., and Huo, Q. (2014b). Predicting detection limits of enzyme-linked immunosorbent assay (ELISA) and bioanalytical techniques in general. Analyst *139*, 439–445.

Zhao, S.-N., Wang, G., Poelman, D., and Voort, P. (2018). Luminescent lanthanide MOFs: a unique platform for chemical sensing. Materials *11*, 572.

Zheng, X., Zhu, X., Lu, Y., Zhao, J., Feng, W., Jia, G., Wang, F., Li, F., and Jin, D. (2016). High-contrast visualization of upconversion luminescence in mice using time-gating approach. Anal Chem. *88*, 3449–3454.

Zhong, Y., Ma, Z., Zhu, S., Yue, J., Zhang, M., Antaris, A.L., Yuan, J., Cui, R., Wan, H., Zhou, Y., et al. (2017). Boosting the down-shifting luminescence of rare-earth nanocrystals for biological imaging beyond 1500 nm. Nat. Commun. *8*, 737.

Zhou, S., Zheng, W., Chen, Z., Tu, D., Liu, Y., Ma, E., Li, R., Zhu, H., Huang, M., and Chen, X. (2014). Dissolution-enhanced luminescent bioassay based on inorganic lanthanide nanoparticles. Angew. Chem. Int. Ed. *53*, 12498–12502.

Zhu, Z., Song, B., Yuan, J., and Yang, C. (2016). Enabling the triplet of tetraphenylethene to sensitize the excited state of europium(III) for protein detection and time-resolved luminescence imaging. Adv. Sci. (Weinh) *3*, 1600146.

Zhuang, T., Lee, H.S., Imperiali, B., and Prestegard, J.H. (2008). Structure determination of a galectin-3-carbohydrate complex using paramagnetism-based NMR constraints. Protein Sci. *17*, 1220–1231.